

## Uncertainties in the Determination of the $W$ Boson Mass

Nicholas Zanata

*Stony Brook High Energy Physics Department (SBHEP)*

### I. Introduction/Abstract

In the standard model<sup>1</sup> of particle physics, the mass of the  $W$  boson,  $M_W$ , is an intrinsic measurement to make with the highest possible precision. The value is correlated with the mass of the top quark,  $m_t$ , and the mass of the Higgs boson,  $M_H$ , in higher order processes of the standard model framework. Because of this, accurate measurements of  $M_W$  and  $m_t$  test the internal consistency of the standard model. For example, comparing the constrained measurements of  $M_H$  to the actual value of the boson not only helps validate the standard model as a coherent whole, but helps further define the properties of the Higgs boson itself. Due to the interrelated nature of the standard model's constituents, understanding  $M_W$  in full detail is of critical importance, especially if we intend to further understand the electroweak portion of the model. The standard model is a primarily predictive tool employed when undertaking experiments in particle physics. An advanced understanding of the subatomic physical world cannot be achieved without completion of the standard model.

The goal of this project is to determine the Parton Distribution Function (PDF) uncertainty in the  $M_W$  measurement at the D0 experiment. Using these PDFs and the  $W$  boson to electron-neutrino decay events generated by ResBos<sup>2</sup>, we study the primary causes of these uncertainties. We do this by using the detector fast simulation, Parametric Monte Carlo Simulation (PMCS). There are four distinct PDFs that we analyze: CTEQ6.6<sup>2</sup>, CT10w, CT10, and CT10[12] where only the up and down quarks are considered. This analysis also helps us understand what additional measurements could be made to improve the PDF uncertainty.

#### I.a. PDF Studies

The process by which  $W$  boson production and decay is simulated is often split into three separate steps, illustrated in Fig. 1 below. Each step represents a portion of the process, and since we cannot measure the  $W$  directly, we are forced to measure the visible momentum components after the  $W$  boson has decayed.

The first step in the simulation represents the role played by PDF set we are using. PDFs are momentum probability distribution functions that characterize the partons (i.e., quarks and gluons) within the proton and antiproton whose collision is being simulated. When the momentum of the protons/anti-protons is sufficiently large as in our situation, then the parton momentum can be considered collinear with the overall proton momentum.

The second step represents a hard interaction. This interaction is simply the collision of two quarks within the protons from step one. This collision produces a  $W$  boson. An up quark and an anti-down quark will produce a  $W^+$ , while a down quark and an anti-up quark will produce a  $W^-$ . Because the up and the down quarks (and their anti-quark pairs) comprise the majority of the reactions producing  $W$  bosons, we also consider a special case in which we focus only on these two flavors. This case is described in more detail below. For our experiment, we use ResBos to simulate  $10^9$  of these production events.

The third step simulates the detector. The  $W$  boson decays too quickly to detect, but we can gather information from studying its decay products. The most common decay products are quark and anti-quark pairs, but decays to leptons also occur. For our experiment, we select certain decay topologies; in the case of a  $W^+$  the selected decay products are an electron (a positron,  $e^+$  in the  $W^+$  case) and an anti-electron neutrino (electron neutrino,  $\bar{\nu}_e$  in the opposite case). Gamma radiation is emitted during the decay process in some cases, which must be accounted for when determining the mass of the  $W$  boson. This step uses the events produced by ResBos in the previous step to obtain results for the transverse momentum ( $p_T$ ), the transverse mass ( $m_T$ ), and the missing transverse energy ( $E_T$ ) from the collision. These provide us with information concerning the  $W$  boson mass by applying the basic principles of conservation of energy and momentum.

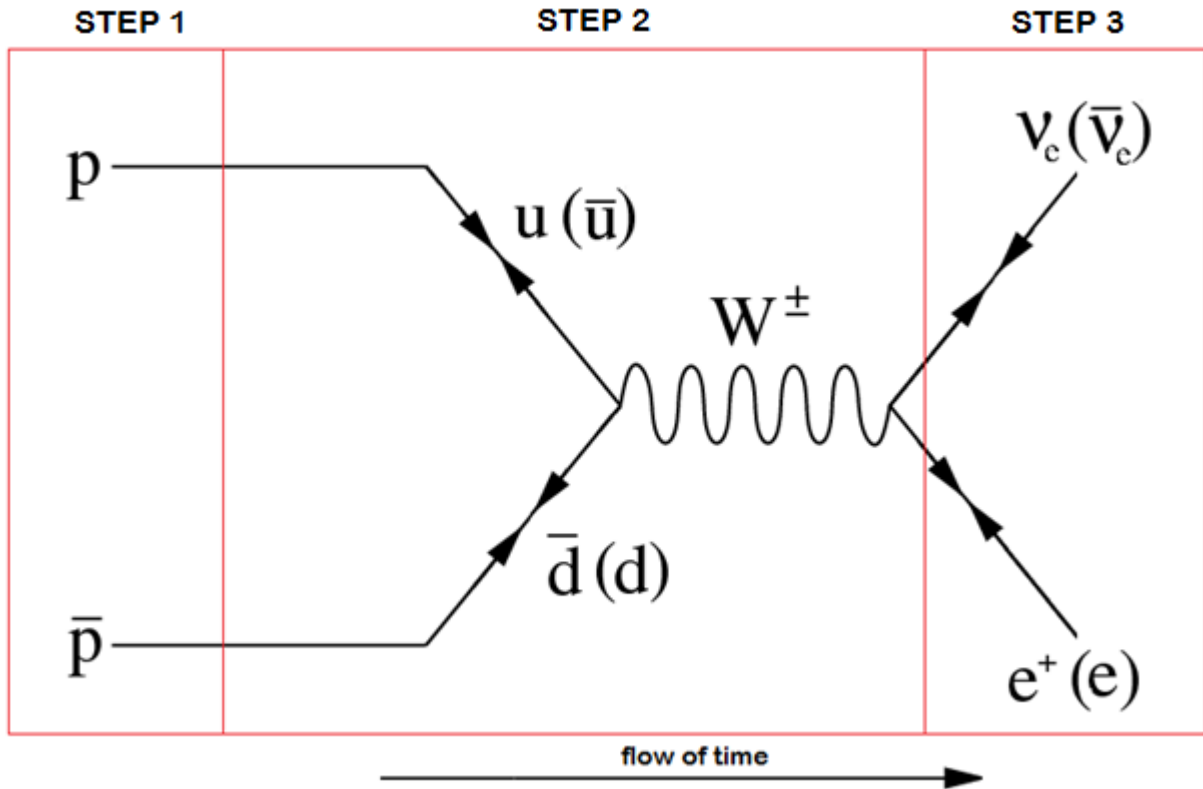


Figure 1: A diagram showing the production and decay of a W boson, with each step described in the text. Both possibilities for forming a W- either with a positive or negative charge- are displayed so the reader can observe the differences. The partons and products in parenthesis represent the case of W.

**I.b.  $M_W$  Studies**

To study the mass of the W boson, we must understand the processes that lead to its creation. We begin with the following equation, taken from the theory of special relativity.

$$[1] (mc^2)^2 + (\vec{p}c)^2 = E^2$$

This is an expression for energy. If we move the momentum term to the right and solve for the mass, we'd have the following expression.

$$[2] m^2 = E^2 - \vec{p}^2$$

We can use this relationship to solve for  $M_W$ . However, an issue arises. It is impossible to measure the energy and z-direction momentum of the quarks in step one which create the W boson for two reasons: the construction of the D0 detector, and the impossibility of determining which quarks collide to form the W boson. If we could hypothetically measure these decay products completely, then this simple method would work. Unfortunately, all we have is the information contained in step three (what the detector actually measures), which we can use to find an expression for the mass. If we represent the energy and momentum of the electron neutrino in step three as  $E_1$  and  $\vec{p}_1$  and the energy and momentum of the electron in step three as  $E_2$  and  $\vec{p}_2$ , then the W boson is represented as follows:

$$[3] E = E_1 + E_2$$

$$[4] \vec{p} = \vec{p}_1 + \vec{p}_2.$$

If the products in step three are the result of decay from the boson in step two, then this relation must be true. Using expression [2], we then have the following equations:

$$[5] M_W^2 = (E_1 + E_2)^2 - (\vec{p}_1 + \vec{p}_2)^2$$

$$[6] M_W^2 = (E_1^2 - \vec{p}_1^2) + (E_2^2 - \vec{p}_2^2) + 2(E_1E_2 - \vec{p}_1\vec{p}_2).$$

Because the mass of the electron and neutrino are small compared to their momentum in W boson decay, the following two terms are negligible: the first term, which is the mass of the electron neutrino, and the second term, which is the mass of the electron. We may ignore these arriving at our intermediate expression for  $M_W$ :

$$[7] M_W = \sqrt{2(E_1E_2 - \vec{p}_1\vec{p}_2)}.$$

We can make one last simplification. The momentum term is a dot product, so we may simplify [7] further:

$$[8] \overline{p_1 p_2} = p_1 p_2 \cos(\theta).$$

And thus:

$$[9] M_W = \sqrt{2(E_1 E_2 - p_1 p_2 \cos(\theta))}.$$

Finally, we get the following expression if we simplify the momentum portion, pulling it outside the parenthesis and again neglecting the electron and neutrino masses for simplicity:

$$[10] M_W = \sqrt{2E_1 E_2 (1 - \cos(\theta))}.$$

Unfortunately this expression cannot be used directly because we cannot measure (or infer, from other decay products) the energy or momentum of the z-component of the neutrino. We need a better way of determining the relevant information to determine  $M_W$  while keeping in mind the construction of the detector we are simulating.

The momentum of the proton and anti-proton beams in step one are characterized by their individual translational components, with respect to x, y, and z. The momenta used in our measurements are those perpendicular to the z-axis, where the z-axis is defined by the proton beam direction in the detector.<sup>3</sup> The choice of this specific basis makes our study of the decay products much simpler. This implies the quantities of importance are those that lie transverse to the z-axis. The protons are moving at speeds on the order of  $c$ , so the z-component of the quark momenta will be enormous compared to the transverse components. We employ the following conventional expression for the transverse momentum.

$$[11] p_t = \sqrt{p_x^2 + p_y^2}$$

If our detector were perfect, then the electron or neutrino transverse momentum distribution would look as shown in Fig. 2.

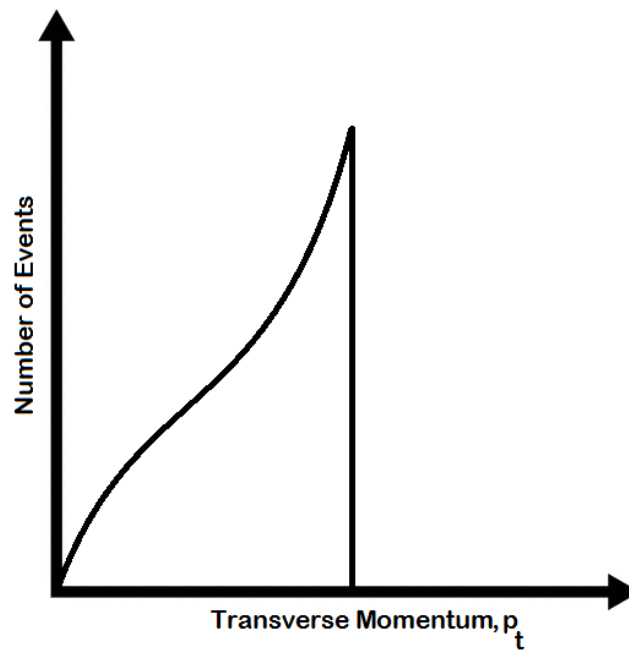


*Figure 2: The “perfect detector” distribution for number of events vs. transverse momentum. In this case we are assuming the measurement of the decay products is perfect and that the W boson has no transverse momentum. The curve falls abruptly to zero at a momentum value corresponding to exactly half of  $M_W$ . It should be noted that the same analysis and subsequent reasoning will follow for the transverse missing energy and the transverse mass; in the case of transverse mass, the edge would fall at exactly  $M_W$ .*

The distribution above falls exactly at the transverse momentum value that corresponds to half of the expected value of  $M_W$ . If we wanted to find  $M_W$  precisely in this perfect situation, this graph would suffice. However, physical reality is not this ideal. Fig. 2 will be replaced by a skewed version of this distribution, the result of a number of factors including the resolution of the detector, the width (related to the lifetime) of the W boson, the W boson transverse momentum, and the occasional emission of photons during the W boson's decay. The width, of the W boson is defined as follows:

$$[12] \text{lifetime} = \frac{\hbar}{\Gamma}.$$

Often, this is set to 1 for simplicity:

$$[13] lifetime = \frac{1}{\Gamma}$$

One last concept remains to be discussed. Due to the construction of the central calorimeter within our detector, there is only a specific range of angles that allow the electrons in step three to be detected. Electron neutrinos are impossible to detect, so our data comes primarily from analysis of the electron that is possible to detect. A cross section of the calorimeter, illustrated in Fig. 3, provides the following geometrical information.

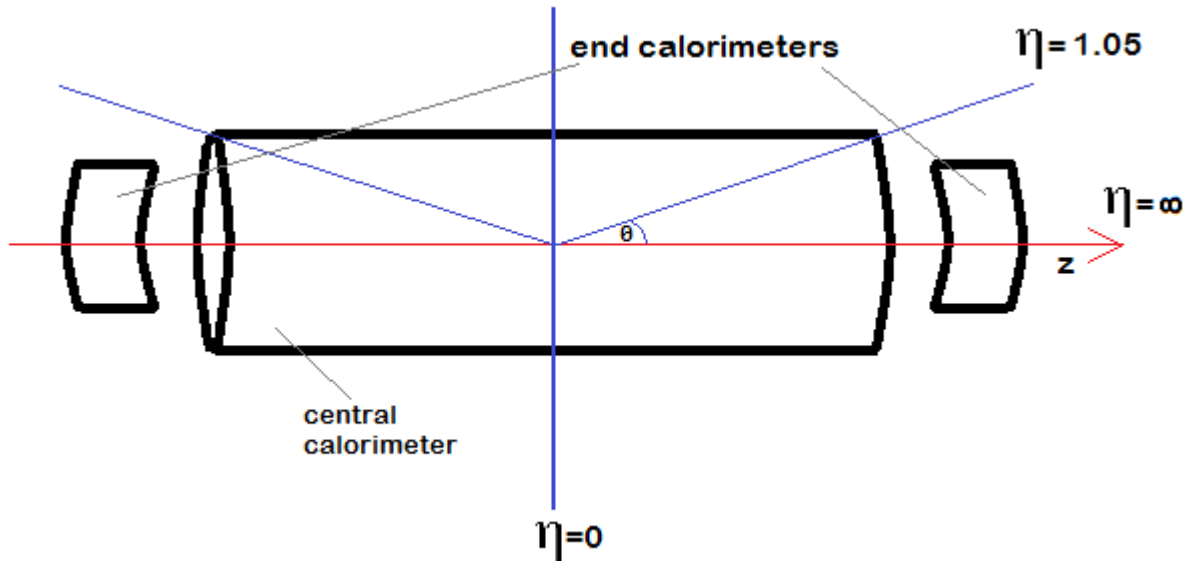


Figure 3: A rough drawing of the calorimeter (not to scale) used for our experiment. The end calorimeters provide hermeticity.

The tangent of theta above is easily defined using standard trigonometry:

$$[14] \tan\theta = \frac{\sqrt{p_x^2 + p_y^2}}{p_z} = \frac{p_t}{p_z}$$

The angle eta, which defines the pseudo-rapidity, is given by:

$$[15] \eta = -\ln \left[ \tan \left( \frac{\theta}{2} \right) \right]$$

Eta is infinite along the z-axis and zero in the direction perpendicular to the proton beams. The usable portion of the central calorimeter corresponds to  $-1.05 < \eta < 1.05$ , and this defines the angle with which we restrict our measurements. Knowing eta provides us with crucial information regarding the momentum and energy of the particle. If eta is well defined, then so is the z momentum component,  $p_z$ . Energy (related to the electron momentum as described earlier) in this case is represented by the equation:

$$[16] E^2 = p_t^2 + p_z^2$$

For a fixed energy value, if the z momentum goes up, then the transverse momentum must go down, and vice versa. Because the energy is also dependent on the momentum of the quarks colliding to produce the W boson, we define a new variable to make measurements of the momenta ratios. We define the following expression:

$$[17] X = \left| \frac{\vec{p}_{quark}}{\vec{p}_{proton}} \right|$$

This quantity will be explained in more detail below.

## II. Programs and Simulations

Thus far we have mentioned the use of programs like the fast detector simulation PMCS and the event generator ResBos for proton anti-proton collision events which together are used to simulate W production. We now describe these programs in more detail before we proceed with presenting our simulated data.

### II.a. Details on the Programs Used

Below is a short summary of the details of each of the main programs used for this experiment.

### *II.a.1 ResBos*

Res Bos, which is an acronym for RESummation for BOSons<sup>2</sup>, is an event generator that simulates the production of the  $W$  for our experiment. As explained above, ResBos simulates proton-antiproton collisions in the Tevatron, and the subsequent decay into an electron and neutrino pair. ResBos also contains a detailed treatment of the gluons radiated from the quarks and anti-quarks that participate in the hard interaction described above. This detail provides us with a prediction for the transverse momentum of the  $W$ . To simulate the radiation of a photon during the decay of the  $W$ , we use the program PHOTOS<sup>3</sup> in conjunction with ResBos. The final result of these two event generators working in conjunction is a list of the electron, neutrino, and photon four-vectors for each simulated  $W$  boson event. These are used as the input to the simulation of our detector, PMCS. By varying the PDF set used when running ResBos, we can study the PDF set's impact on the  $W$  boson mass determination. In addition to using different PDF sets, the uncertainty from a given PDF set is determined by using the error sets provided by the groups that determine the PDFs.

### *II.a.2 Running PMCS*

PMCS is a fast detector simulation of the D0 detector. It uses the events generated by ResBos in tandem with PHOTOS to simulate the effects of the detector itself on the final portion of our interaction, which are the decay products of the  $W$ . Each event utilizes the electron, neutrino, and photon four-vectors from ResBos and a specific set of parametrizations to determine how the electron energy and missing transverse energy,  $E_t$ , are measured by the detector. The output of PMCS is thus a prediction of  $p_t$ ,  $m_t$ , and  $E_t$  that can then be compared to the data.

### *II.a.3 WZfitter*

WZfitter is a program that compares the three distributions predicted by PMCS to the ones measured directly with the detector, or ones produced by variations of PDF or detector parametrizations. WZfitter uses PMCS  $m_t$ ,  $p_t$ , and  $E_t$  distributions for a certain choice of  $M_W$  as input. The output is thus a value of  $M_W$  which reproduces the observed data most accurately. We use WZfitter in this experiment to estimate the systematic uncertainties of our procedural approach. For this report, we compare distributions predicted from PMCS to another PMCS simulation, varying the PDF only. If we compare the output of WZfitter for events generated using a PDF uncertainty variation with the events generated with the known  $M_W$  that the ResBos simulation was generated with (and with nominal PDF settings), we have a measure of the propagated uncertainty from PDFs on our experimental results. PDF sets are defined by a multitude of parameters, so we repeat the procedure multiple times for each variation by the groups that produced them and sum all the variations in quadrature.

$$[18] \frac{1}{1.6} \sum_i \sqrt{\frac{1}{2} (M_+ - M_-)^2}$$

The factor 1.6 is necessary since the CTEQ group provides variations at 90% confidence level (CL), while here we will report uncertainties at 68% CL. This equation will be refined further below.

## **III. Data Analysis and Presentation**

Using the results from ResBos, the PMCS simulated detector, and WZfitter, we can analyze the impact of potential uncertainties and highlight their affect on our determination of  $M_W$ . Each PDF uncertainty is determined by the combined use of ResBos, PMCS, and WZfitter. This produces three numerical measured quantities that are used to determine  $M_W$ . These quantities are a distribution of yield (the number of selected events) vs. electron  $p_t$ , a distribution of yield vs.  $E_t$ , and a distribution of yield vs.  $m_t$ . The transverse momentum distribution is shown in Fig. 4, the transverse mass in Fig. 5, and the missing transverse energy in Fig. 6. Each figure shows the respective results for the central values of the four PDF sets we consider.

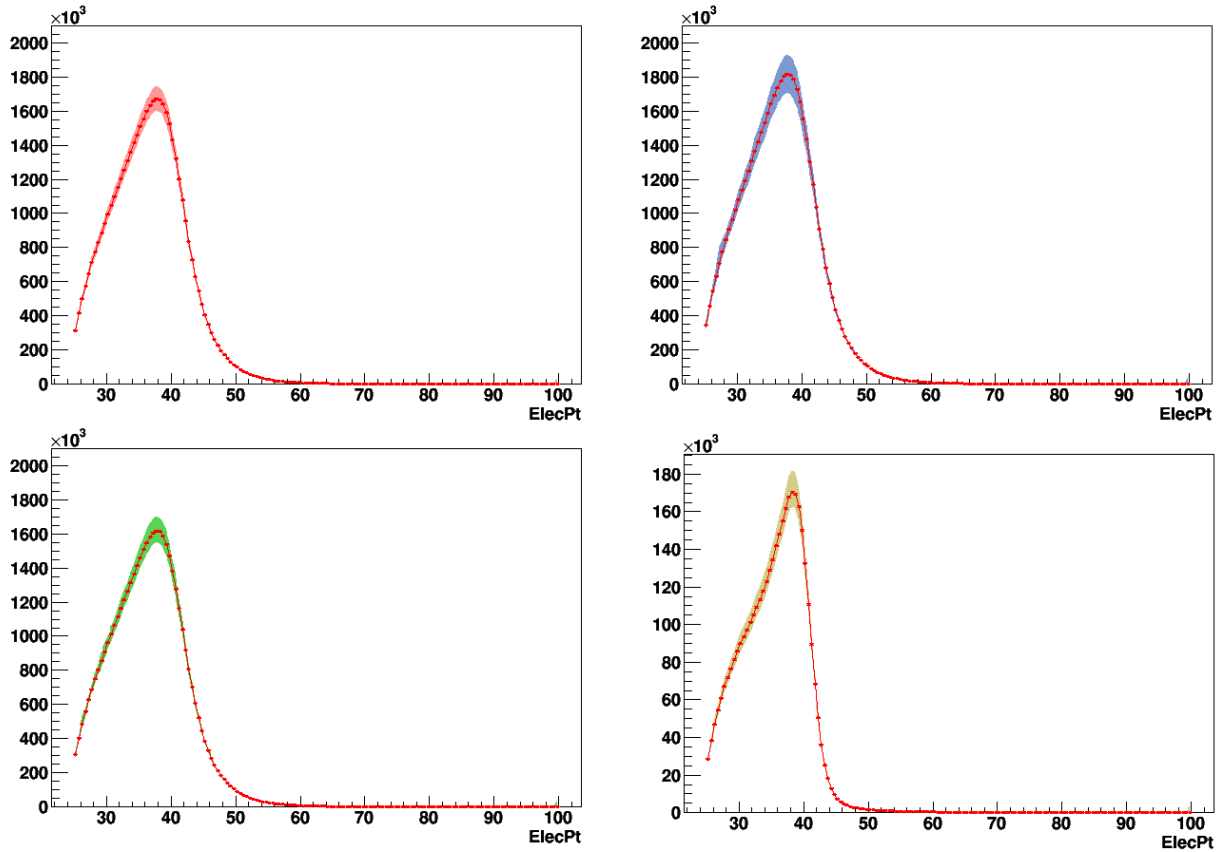


Figure 4: Electron transverse momentum ( $p_t$ ) distributions for the four PDF sets. The red band (upper left) is for CTEQ6.6, the blue band for CT10w (upper right), the green band for CT10 (lower left), and the brown band for CT10 [12] (lower right). The axes are uniform for all these plots with the exception of CT10 [12]. The red curve within each band is the statistical uncertainty of our PDFs.

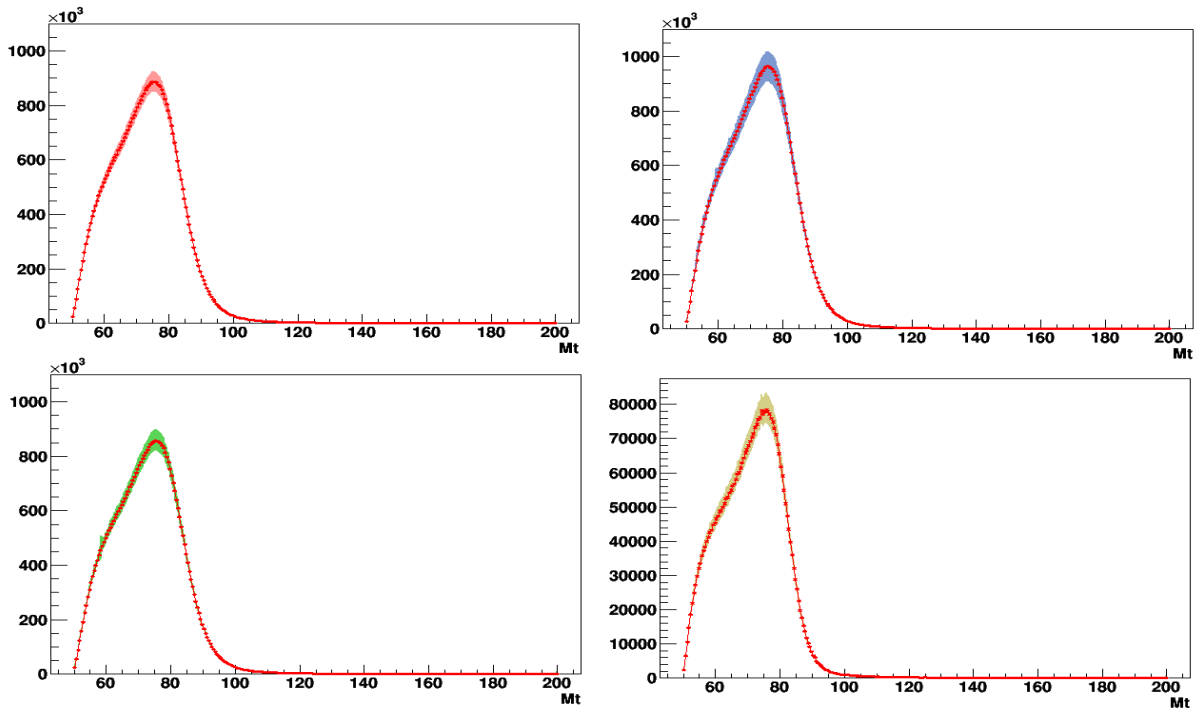


Figure 5: The transverse mass ( $m_t$ ) distributions for each of the four PDF sets. The same color coding applies as was discussed in the caption below Fig. 4.

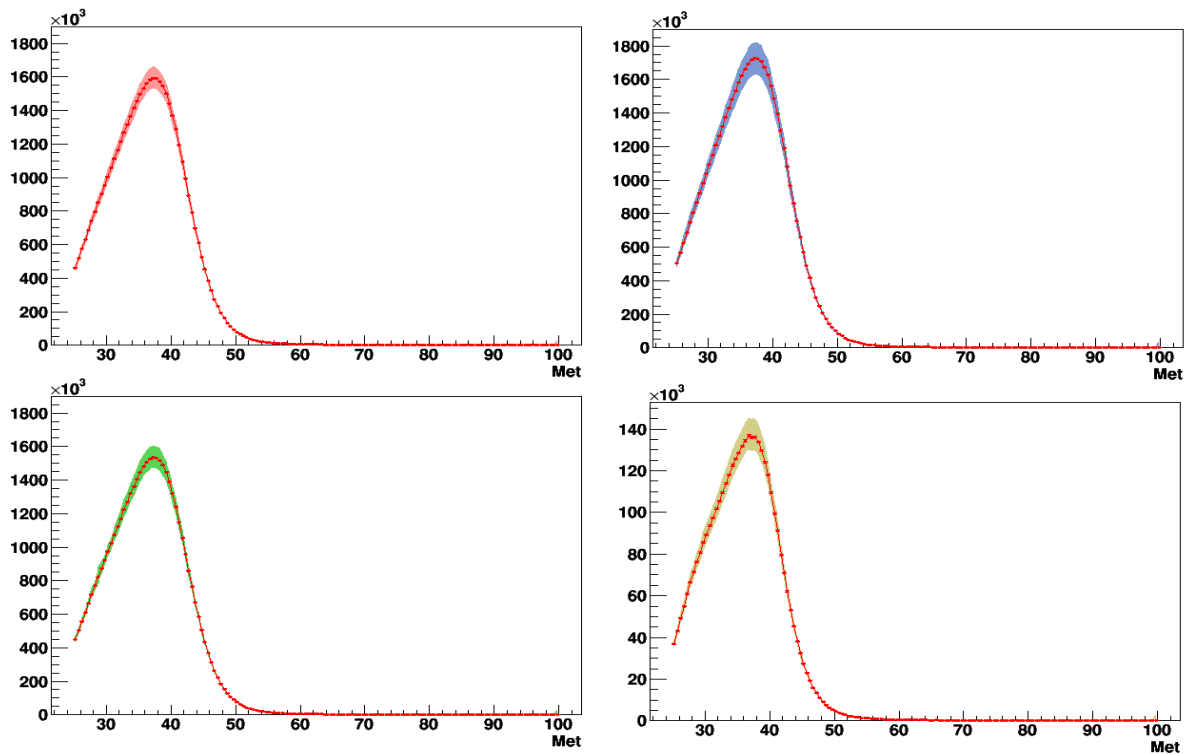


Figure 6: The missing transverse energy ( $E_t$ ) distribution for each of our four PDF sets. The same color coding applies as was discussed in the caption below Fig. 4.

The bands around each histogram show the total PDF uncertainty and are produced when PMCS is run. Each PDF set provides uncorrelated positive and negative one standard deviation uncertainties. These uncertainties must be carried forward in our calculations. There are 44 uncorrelated (i.e., found as eigen-values from a matrix diagonalization) uncertainties for CTEQ6.6, and one additional one corresponding to the central (also known as the 0<sup>th</sup>) value, raising the total to 45. For CT10w, CT10, and CT10 [12], there are 52 values, with a 53<sup>rd</sup> representing the central value. CTEQ6.6 thus has 22 eigen-values, while the CT10w, CT10, and CT10[12] have 26 eigen-values, where an eigenvalue-pair is simply a pair of the positive and negative uncertainties from a single uncertainty source, defined above and in equation [18] as  $M_+$  and  $M_-$ .

It is also important to note that, as discussed previously, the rightmost edge of each distribution is not perfectly vertical; however, as can be seen above, the values for  $E_t$  and  $p_t$  fall roughly near  $M_W/2$  with the error band peaking in width at the topmost portion of the curve and falling off very sharply to the right. In the case of  $m_t$ , as predicted, the right edge occurs near  $M_W$ . In our studies, the simulated value for  $M_W$  will be taken as:

$$M_W = 80.419 \text{ GeV}$$

Each eigenvalue-pair for each PDF set contributes uncertainty. Of the 22 pairs in CTEQ6.6 and the 26 pairs in CT10w, CT10, and CT10 [12], some contribute more to the overall error determination than others. This can be visualized more succinctly in Fig. 7, which shows specific eigenvalue-pair deviations from the central value.

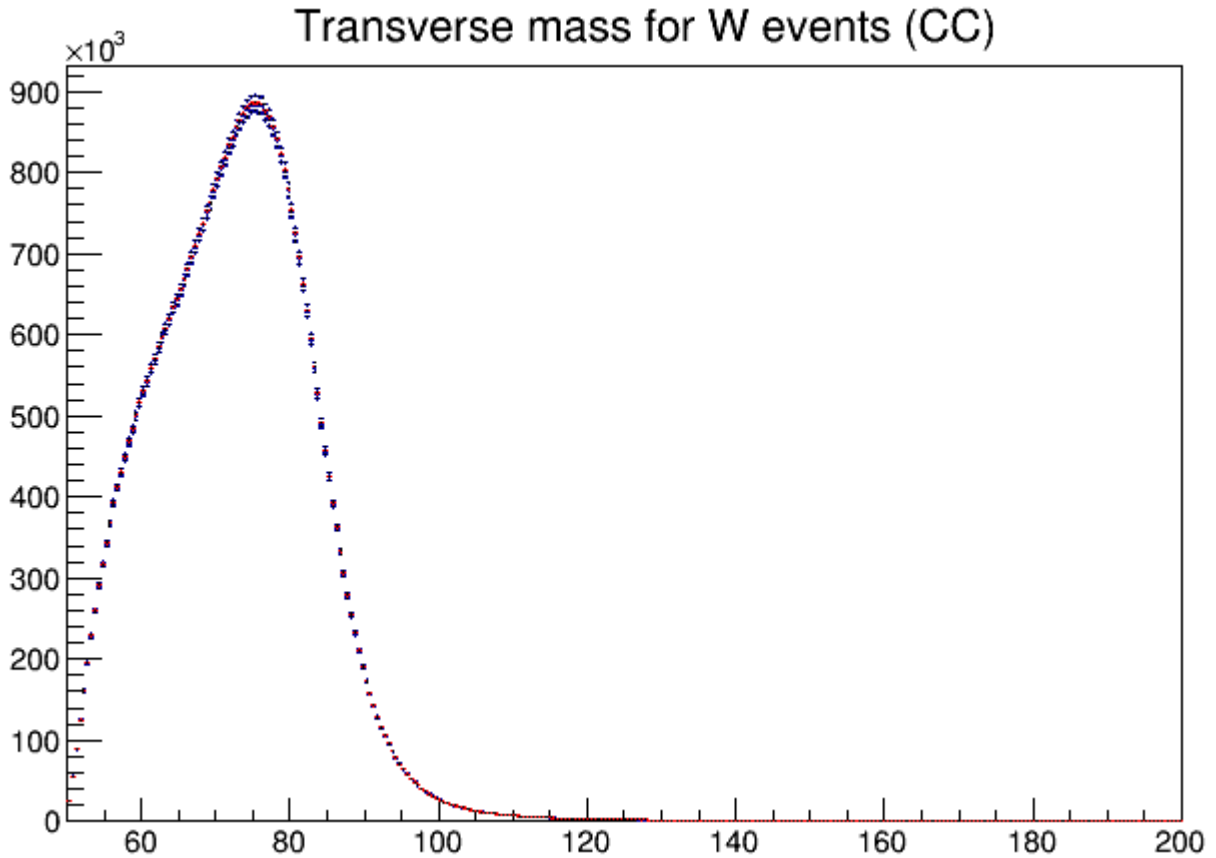


Figure 7: This is a graphical example that utilizes CTEQ6.6's transverse mass. The red distribution represents the central value, while each blue distribution represents a specific eigenvalue-pair which deviates from the central value. Similar results can be shown for transverse momentum and missing transverse energy for the other PDFs.

The red points above represent the central value, while each series of blue points represent the various distributions arising from other PDF eigen-values. Each eigenvalue-pair deviates from the central one by a certain amount; summing the average value of these deviations in quadrature yields the bands shown in Figs. 4 to 6.

### III.a. Final Results

Each individual eigenvalue-pair contributes a certain amount of uncertainty to our determination of  $M_W$ . These values are dealt with in pairs; if one half of the pair contributes some positive uncertainty value, then its partner will contribute an equal and opposite negative value. The most natural question that follows from this is which eigenvalue-pair contributes the most uncertainty to our overall determination? When we plot the uncertainty from each eigenvalue-pair individually we find the results shown in Fig. 8.



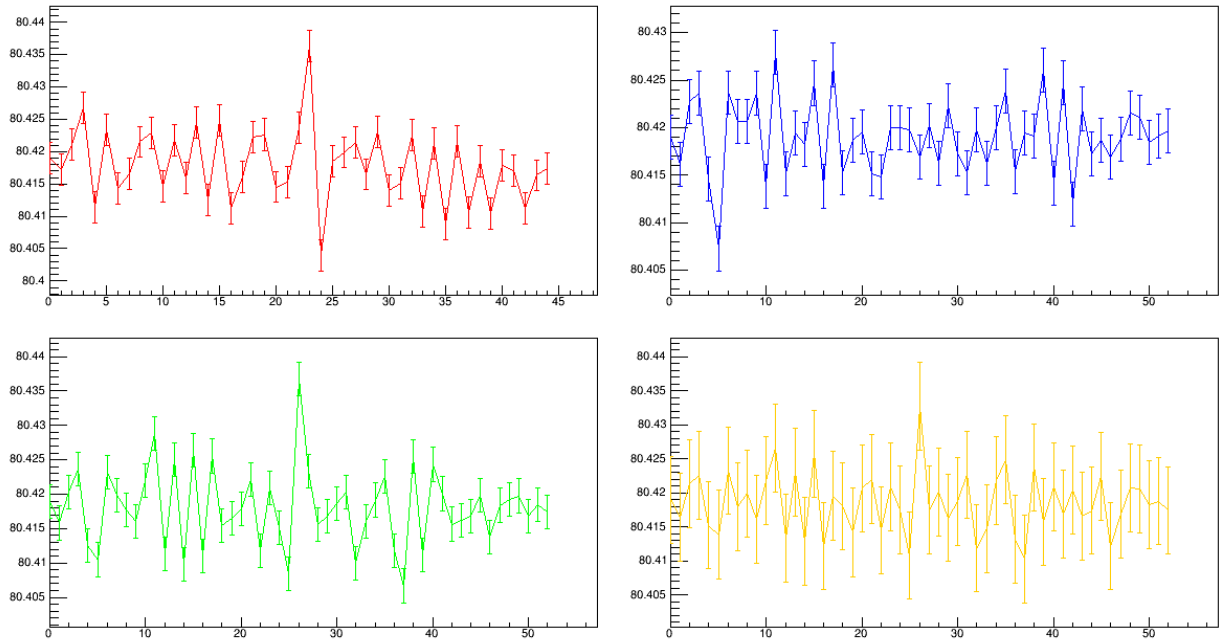


Figure 8: Errors on  $M_W$  arising from PDF variations are shown in the graphs above. The central value lies on the y-axis, while variations are plotted for each individual PDF; the x-axis is the PDF eigenvalue-pair number. Since these come in pairs, each consequent point is equally spaced above and below the central value in increments of two. Red represents CTEQ6.6 (upper left), blue CT10w (upper right), green CT10 (lower left), and orange CT10 [12] (lower right).

Each PDF set has distinct pairs that are exceptional outliers. These pairs contribute far more variation in our determination of  $M_W$  than the other pairs. These plots also highlight an additional source of uncertainty in finding  $M_W$  that we must consider at length. The uncertainty discussed thus far has involved our PDF sets and the uncertainty propagated when we run ResBos and PMCS. There is a second source of uncertainty- purely statistical in nature- that must also be accounted for. Whereas the PDF uncertainty is easily found by measuring the difference between the central value and the value in question, the statistical uncertainty is found by measuring the magnitude of the error bars on each individual point. The formula for the uncertainty on each eigenvalue-pair is expressed in equation [18] above, but it can be rearranged in the following way.

$$[19] \sum_i \frac{(M_+^i - M_-^i)^2}{10.82}$$

In this case, the index  $i$  simply denotes which eigenvalue-pair we are considering;  $M_+$  is the positive uncertainty and  $M_-$  is the negative uncertainty. We then sum over the entirety of our PDF set to obtain some propagated error value, finally taking the square root of this to find the total PDF uncertainty.

$$[20] \sigma_{PDF} = \sqrt{\sum_i \frac{(M_+^i - M_-^i)^2}{10.82}}$$

The statistical uncertainty is found by using the following formula:

$$\frac{\delta\sigma_{PDF}}{\delta M_{\pm}^i} = \frac{1}{\sigma_{PDF}} * \frac{(M_+^i - M_-^i)}{10.82} * \delta M_{\pm}^i.$$

Squaring these expressions, moving the  $\delta M_{\pm}^i$  to the right, and summing over the index  $i$  again, we then have:

$$\delta\sigma_{PDF}^2 = \frac{1}{\sigma_{PDF}^2} * \sum_i \frac{(M_+^i - M_-^i)^2}{10.82^2} * (\delta M_+^{i^2} + \delta M_-^{i^2}).$$

This expression simplifies as follows:

$$[21] \delta\sigma_{PDF} = \frac{1}{10.82\sigma_{PDF}} \sqrt{\sum_i (M_+^i - M_-^i)^2 * (\delta M_+^{i^2} + \delta M_-^{i^2})}.$$

In this case, the symbol  $\delta$  represents the statistical uncertainty on our PDF uncertainty, which is what the error bars on each point represent. Each has statistical uncertainty in the positive and negative direction, which must be summed over the index to cover our entire range of eigen-values.

*III.a.1. Overall Uncertainties*

The uncertainties we have been discussing are summarized in Tables 1 and 2. Statistical error will be noted with the nomenclature “stat,” and it will be added in quadrature to the PDF uncertainty. Table 1 summarizes the number of events generated in each PDF version, while Table 2 summarizes the total uncertainties we have discussed in the section above.

*Table 1  
Each PDF set and the number of events and eigen-values.*

PDF Version	Number of Events	PDF Set Eigen-values
CTEQ6.6	$3.78 \times 10^7$	45
CT10w	$4.11 \times 10^7$	53
CT10	$3.65 \times 10^7$	53

*Table 2  
Each PDF set and it’s uncertainty, including the statistical uncertainty on the result for the transverse mass, momentum, and missing energy.*

Version	$\Delta m_t(\text{MeV})$	$\Delta p_t(\text{MeV})$	$\Delta E_t(\text{MeV})$
CTEQ66	$15.50 \pm 1.04(\text{stat})$	$21.98 \pm 1.09(\text{stat})$	$16.73 \pm 1.17(\text{stat})$
CT10w	$11.38 \pm 0.99(\text{stat})$	$26.23 \pm 1.04(\text{stat})$	$21.85 \pm 1.12(\text{stat})$
CT10	$16.80 \pm 1.05(\text{stat})$	$24.82 \pm 1.10(\text{stat})$	$18.94 \pm 1.19(\text{stat})$
CT10[12]	$13.33 \pm 2.77(\text{stat})$	$11.15 \pm 2.15(\text{stat})$	$18.64 \pm 3.72(\text{stat})$

The uncertainties displayed in Tables 1 and 2 coincide with the data we saw in Fig. 8. The statistical error on the CT10[12] data is much larger because far fewer events were generated for this case than for the others. In addition, the error bars on each of the other PDF versions are roughly similar in magnitude because of the similar number of events generated for each set.

More analysis is needed to understand the uncertainty on each PDF version. The error bounds in Fig. 8 can also be represented using a different type of plotting method which highlights the proton’s X dependence, where X is defined in equation (17). We will also use a new parameter: the correlation with the PDF data. This function defines the PDF induced correlation with the data in question, which is then represented by a correlation coefficient. Coefficients with an absolute value close to one indicate the data is particularly powerful with regards to influencing the overall uncertainty on  $M_W$  at that specific X value. This method helps us understand where certain momentum ratios become more (or less) responsible for contributing to our overall uncertainty. The X ratio is placed on the x-axis, with the coefficient placed on the y-axis. We will also document the PDF uncertainty and the X uncertainty, both centered at zero.

Because W boson production involves an up and a down quark, our analysis will plot the correlation, the PDF uncertainty, and the X uncertainty with respect to the u/d ratio. Of course, we could produce similar data for only one flavor, but this information is significantly less valuable; a W can only be produced with the collision of two separate quark flavors, and the up and down are overwhelmingly probable.

*III.a.2. CTEQ6.6*

The first PDF version we analyze in detail is CTEQ6.6. As was previously mentioned, CTEQ6.6 only uses 44 eigen-values. Entries are all centered about a central value, bringing the total to 45 eigen-values. We interpret the data in pairs. There are 22 eigenvalue-pairs to analyze in this version, as can be seen in Figs. 8 and 9. Fig. 9 shows the results for the  $m_t$  distribution.

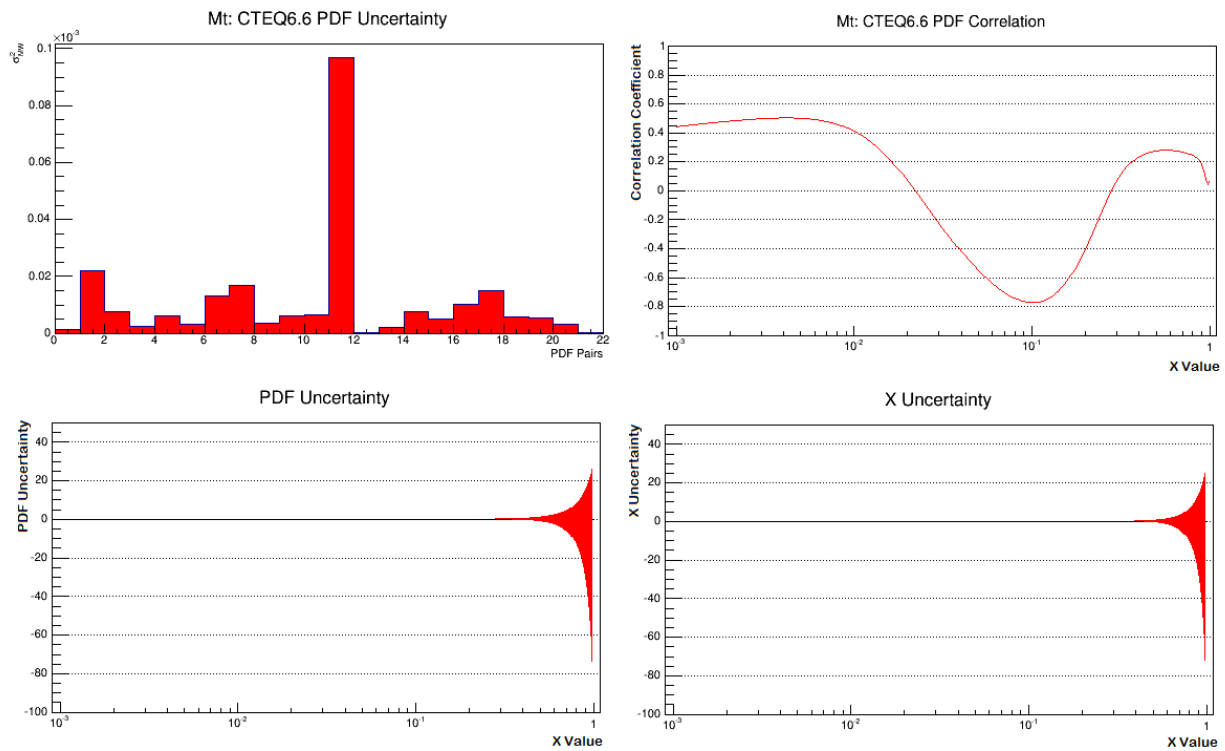


Figure 9: Results derived from the transverse mass distribution generated with CTEQ6.6. Starting from the top left and moving clockwise, we have a) the uncertainty as measured by eigenvalue-pair, with the uncertainty for each pair represented by a specific bar, b) the correlation coefficient, which relates the variable  $X$  to the correlation it has with regards to the fitted  $M_W$  value (the ability such an  $X$  value has to alter our measurements), c) the PDF uncertainty with respect to  $X$ , and d) the  $X$  uncertainty as graphed with respect to  $X$  itself.

CTEQ6.6 has one very obvious pair that dominates the uncertainty in our simulation. Eigenvalue-pair 12 contributes the dominant uncertainty to our data and thus contributes the largest uncertainty measurement on  $M_W$ . The correlation coefficient peaks in value around  $X=0.1$ , shown by a sharp dip in the curve that comes to a maximum excursion value of roughly  $-0.8$ . At this point, the corresponding  $X$  ratio will strongly influence the uncertainty of our data; we must pay closer attention to this point as a result. This trough stretches between  $X$  values of 0.07 to 0.2, giving us a wide range to analyze.

The PDF uncertainty, however, is much different. This uncertainty in the PDF instance grows consistently starting near an  $X$  value of 0.2. In the  $X$  instance this begins near an  $X$  value of 0.3. Before these values, the uncertainty in both instances is a very thin band. Our area of interest would of course be near the  $X$  value corresponding to a large correlation coefficient, but it seems at the point in question, the uncertainty is small, on the order of  $-0.1$  to  $0.1$  in the PDF uncertainty case and on the order of  $-0.005$  to  $0.005$  in the  $X$  uncertainty case. Evidently, then, the uncertainty on these two measurements does not coincide with the correlation coefficient very strongly. It should be noted that the PDF uncertainty also seems to grow in value at a much faster rate than the  $X$  uncertainty as the value of  $X$  increases. This growth reaches a maximum for both at  $X=1$ .

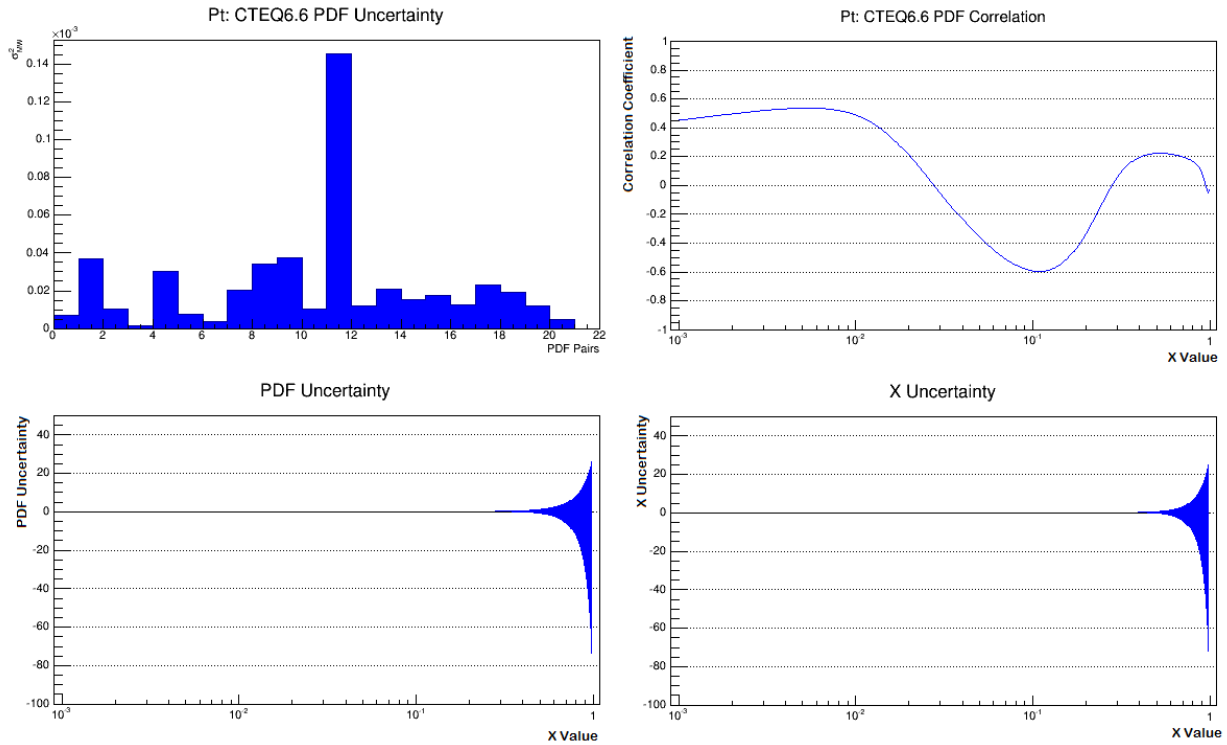


Figure 10: Results derived from the transverse momentum distribution generated with CTEQ6.6. Starting from the top left and moving clockwise, we have a) the uncertainty as measured by eigenvalue-pair, with the uncertainty for each pair represented by a specific bar, b) the correlation coefficient, which relates the variable X to the correlation it has with regards to the fitted  $M_W$  value (the ability such an X value has to alter our measurements), c) the PDF uncertainty with respect to X, and d) the X uncertainty as graphed with respect to X itself.

If we analyze the transverse momentum, we come to similar conclusions with regards to CTEQ6.6 as we did for the transverse mass. Again, the twelfth pair is a very obvious outlier, skewing our data significantly. The correlation coefficient, while reaching a maximum value at the same X number, is not as large: in this case, roughly -0.6 between values of roughly 0.07 and 0.2. Analyzing the same regime in the PDF uncertainty and X uncertainty graphs reveals that the uncertainty bands do not increase at all or show any oddities at this particular X value range. This implies that the correlation coefficient does not correspond to any important increase in the PDF or X uncertainties, despite its prominence at the specified X range. The graphs in this instance increase exponentially- the PDF uncertainty again much faster than the X uncertainty- until reaching a maximum near an X value of 1. Interestingly, and as can be seen above, the negative portion of the PDF and X uncertainties is much larger than the positive portion, showing a decidedly asymmetrical shape.

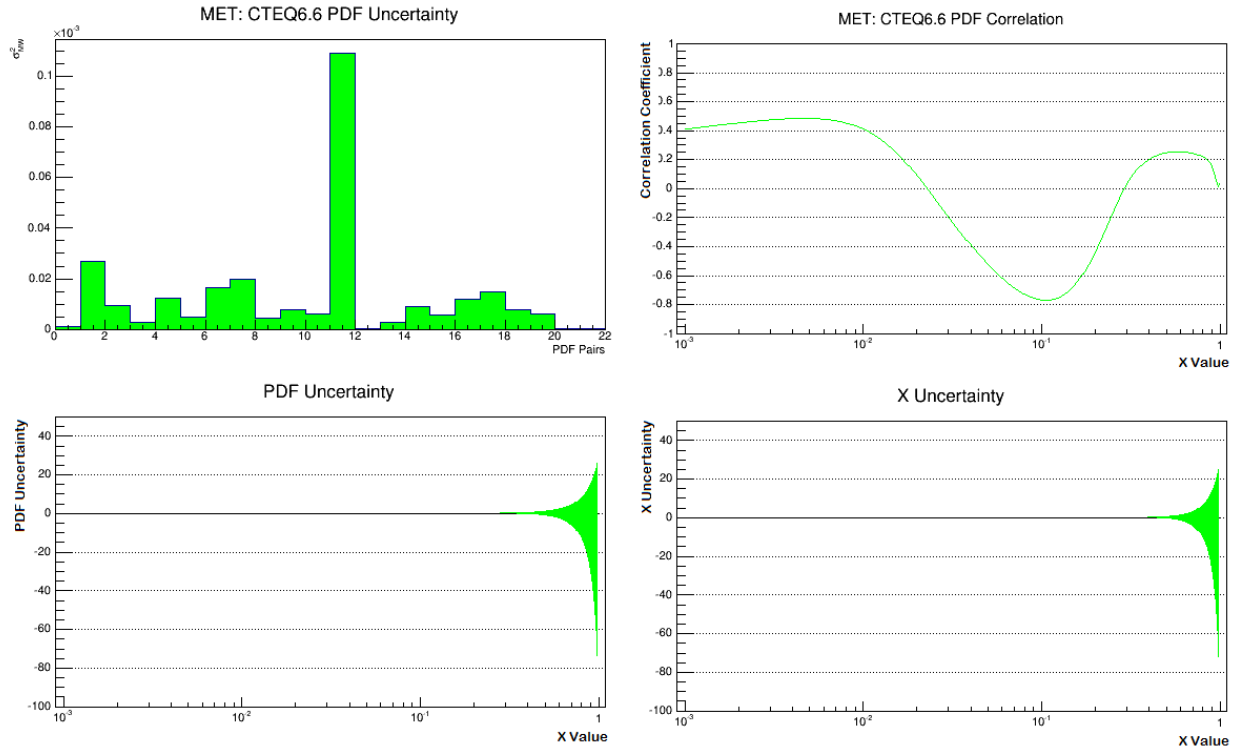


Figure 11: Results derived from the missing transverse energy distribution generated with CTEQ6.6. Starting from the top left and moving clockwise, we have a) the uncertainty as measured by eigenvalue-pair, with the uncertainty for each pair represented by a specific bar, b) the correlation coefficient, which relates the variable X to the correlation it has with regards to the fitted  $M_W$  value (the ability such an X value has to alter our measurements), c) the PDF uncertainty with respect to X, and d) the X uncertainty as graphed with respect to X itself.

These graphs are again strikingly similar to the ones presented above. In this case, the outlier pair is again clearly 12. The correlation coefficient is also near the same X value, and has a maximum excursion value of -0.8, matching the transverse mass more closely than the transverse momentum.

It would appear CTEQ6.6 is quite uniform. Of all the quantities we have chosen to measure, we have attained results that are startlingly similar across the board. These are summarized in Table 3.

Table 3

CTEQ6.6 data for the transverse mass, momentum, and missing energy. The data is divided into sections based on the data shown in Figs. 9-11.

Quantity	Outlier PDF pair(s)	Max value correlation coefficient and position (abs. value)	PDF Uncertainty behavior at correlation coefficient position	X Uncertainty behavior at correlation coefficient position	Magnitude of PDF uncertainty band at correlation coefficient position	Magnitude of X uncertainty band at correlation coefficient position
$m_t$	12	-0.8 at X=0.1	Narrow band, increases exponentially. No obvious dependence at or near X=0.1	Narrow band, increases exponentially. No obvious dependence at or near X=0.1	Roughly -0.1 to 0.1.	Roughly -0.005 to 0.005.
$p_t$	12	-0.6 at X=0.1	Narrow band, increases exponentially. No obvious dependence at	Narrow band, increases exponentially. No obvious dependence at	Roughly -0.1 to 0.1.	Roughly -0.005 to 0.005.

			or near X=0.1	or near X=0.1		
$E_t$	12	-0.8 at X=0.1	Narrow band, increases exponentially. No obvious dependence at or near X=0.1	Narrow band, increases exponentially. No obvious dependence at or near X=0.1	Roughly -0.1 to 0.1.	Roughly -0.005 to 0.005.

III.a.3. CT10w

Unlike CTEQ6.6, CT10w has 53 eigen-values, with 52 of them combining for a total of 26 eigenvalue-pairs and the last one providing the central value. There are thus 26 parameters in question, unlike the 22 for CTEQ6.6, making CT10w more accurate than its predecessor. CT10w also takes into account the W charge asymmetry<sup>4</sup>, further improving the accuracy of this PDF set. As in CTEQ6.6, CT10w will be analyzed by looking at the transverse momentum, missing energy, and mass. We begin with the transverse mass, the results of which are shown in Fig. 12.

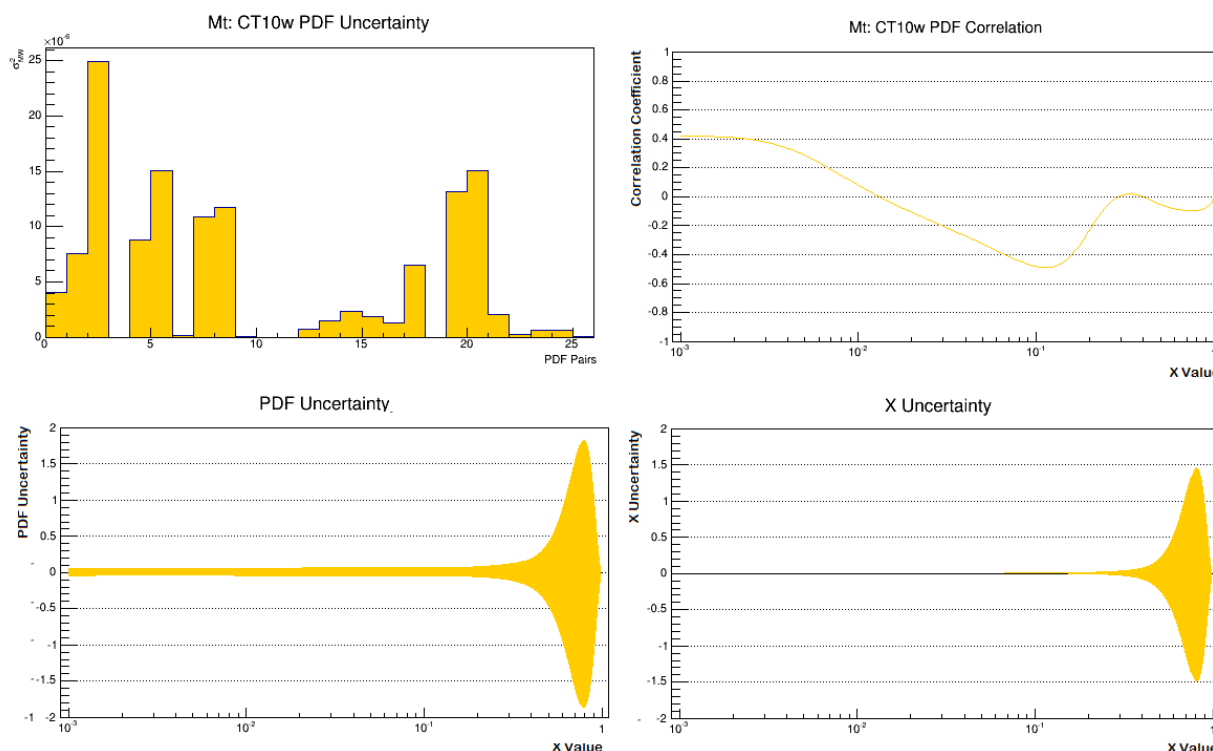


Figure 12: CT10w, with the same data presented for this situation as was done above for CTEQ6.6. There are more bars in the first graph, corresponding to a larger number of uncertainty eigenvalue-pairs.

In this case there is no overwhelming outlier pair. A variety of eigenvalue-pairs do contribute more to our overall uncertainty than others, with eigenvalue-pair 3 being the highest. Eigenvalue-pairs 6 and 21 are also large. The PDF correlation is also much more ambiguous. In magnitude, it is much smaller than the coefficients for CTEQ6.6 in the  $m_t$  case. A gentle slope downward from a coefficient of 0.4 reaches a maximum excursion value at -0.5, slightly past X=0.1. This value then increases to a coefficient of roughly 0 near X=0.3. This change in maximum excursion value – from -0.8 in CTEQ6.6 to -0.5 in CT10w – is telling. The correlation coefficient has changed by 0.3, which indicates that the CTEQ6.6 transverse mass contributes much more uncertainty to  $M_W$  in that PDF set compared to this PDF set. The PDF uncertainty in the lower left is also much thicker in width than the CTEQ6.6 case. The value stretches from -0.05 to 0.05 until the correlation coefficient reaches its lowest point, -0.5. At this value, the band begins to increase exponentially, reaching a maximum that brings the band to a value of -1.9 to 1.9 at X=0.8. At this value, the correlation coefficient shows no particularly interesting behavior; the PDF uncertainty drops off to zero very sharply after X=0.8, but not abruptly as was seen in CTEQ6.6. The X uncertainty is again noticeably smaller than the PDF uncertainty, as was observed above. The band begins with a value of -0.06 to 0.06; the band also seems to inflate before the correlation coefficient reaches its largest value. The X uncertainty band reaches a maximum of -1.5 to 1.5 again at X=0.8, dropping off much faster than the PDF uncertainty.

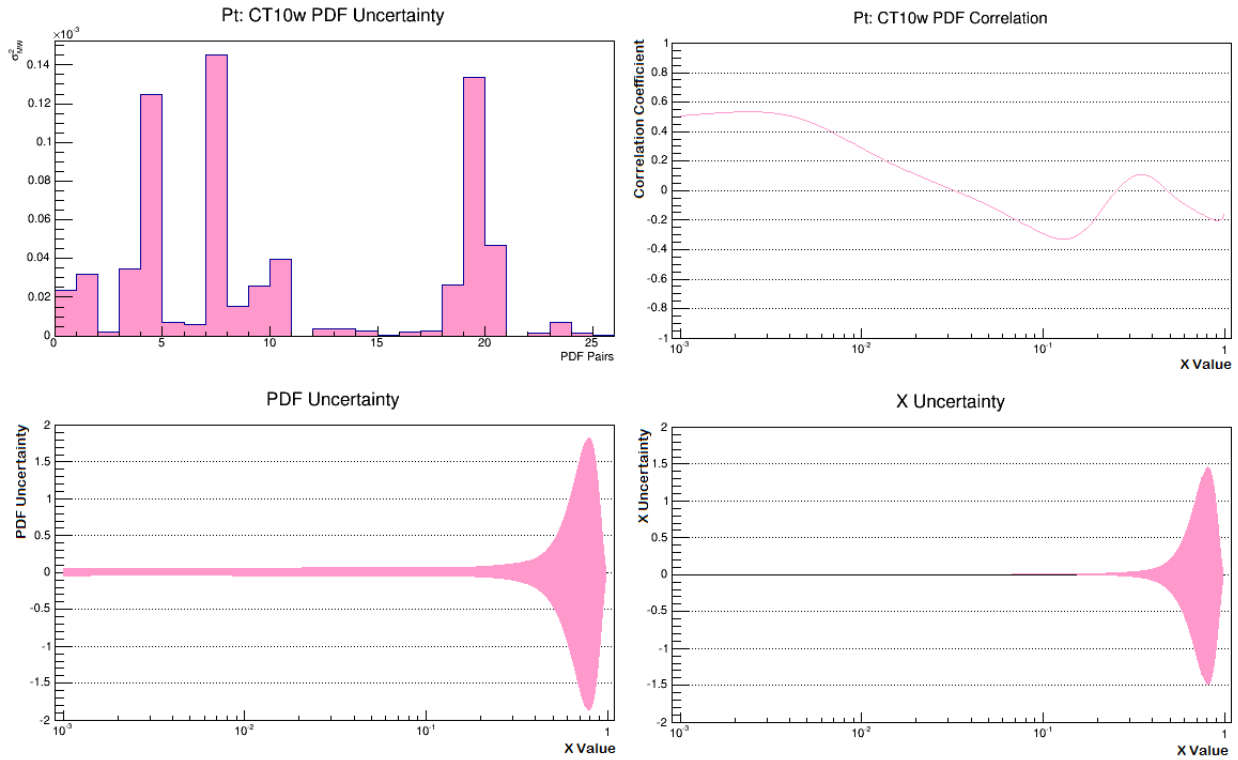


Figure 13: CT10w in the transverse momentum case.

There are significant differences in the PDF eigenvalue-pairs that are larger than their neighbors in the transverse momentum case. For CT10w, these eigenvalue-pairs are 5, 8, and 20, with 8 being the largest. This implies that different variables in our experiment will affect our determination of  $M_W$  when we observe  $p_t$  as opposed to  $m_t$ . The correlation coefficient is a bit more complex here. Our maximum value is attained very near to the beginning- roughly 0.5 at  $X=0.003$ . This value slopes downward rapidly, reaching a value of -0.3 at roughly  $X=0.1$ . The coefficient then increases rapidly, reaching a peak at roughly 0.1 at  $X=0.3$ .

However, there is again not an obvious relationship between a large correlation coefficient and the PDF and X uncertainties. If we consider the maximum to be near  $X=0.003$ , then we see that the PDF uncertainty fluctuates, actually reaching a minimum near the aforementioned correlation coefficient. This undulation continues until we reach slightly past  $X=0.1$ , the point where the correlation coefficient reaches another local maximum. At this point, the band increases exponentially until it hits  $X=0.8$ , where the band stretches from -1.9 to 1.9 in magnitude. It then drops very rapidly until we reach  $X=1$ , where the band disappears.

The X uncertainty is much different. The band remains constant in thickness (a magnitude of -0.0005 to 0.0005) until we reach  $X=0.003$ . At this point- which coincides with the correlation coefficient's maximum- the X uncertainty begins to increase exponentially, at a much quicker rate than the PDF uncertainty. It reaches a maximum at  $X=0.8$ , with a magnitude from -1.5 to 1.5. As expected, it drops off very rapidly to 0 at  $X=1$ .

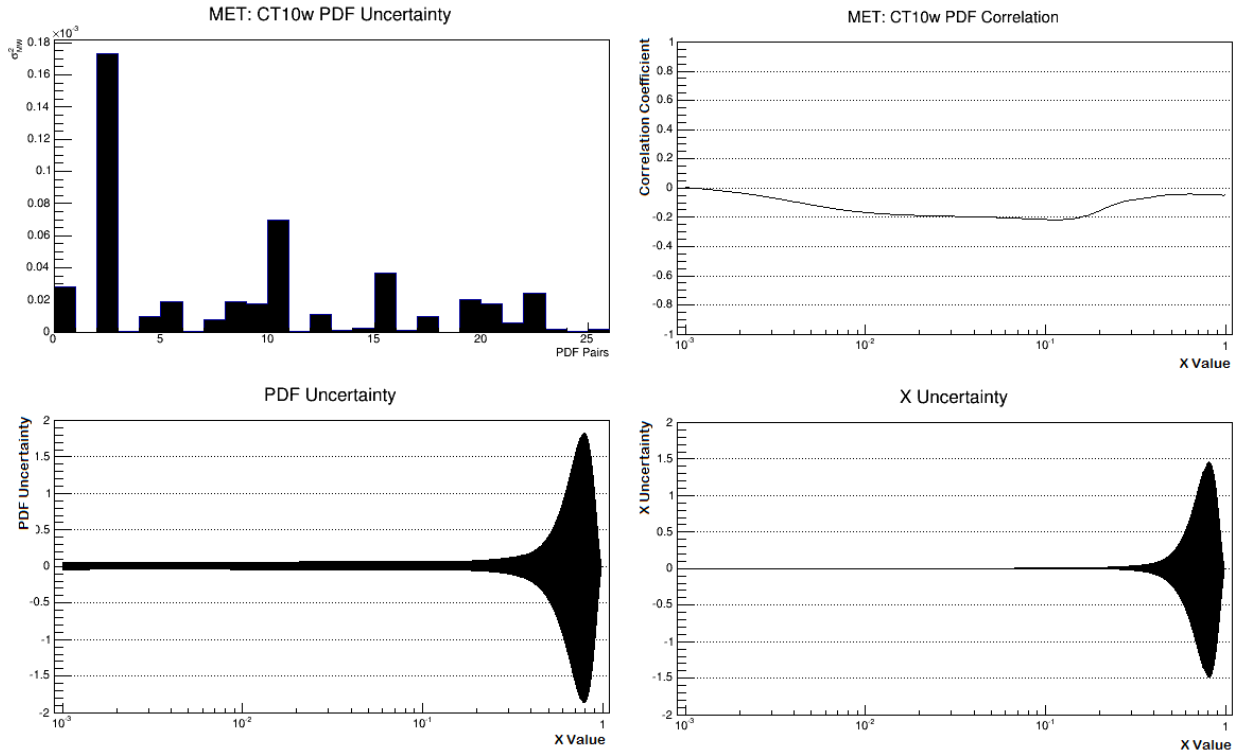


Figure 14: CT10w in the missing transverse energy case.

There is one obvious outlier eigenvalue-pair for  $E_t$ . This is eigenvalue-pair 3, which exceeds the value of the others by a large amount. A second outlier corresponds to eigenvalue-pair 11. The correlation coefficient in this case is surprisingly flat. There is no point where the correlation coefficient is largest. However, if we zoom in, we see there is a very shallow maximum value at roughly  $X=0.1$ , where the coefficient reaches a maximum excursion value of  $-0.2$ . The same undulation as was observed in the transverse momentum for the PDF uncertainty can again be observed here, and when we reach the X value in question that corresponds to our correlation coefficient being at a maximum, the band again starts to increase exponentially until we reach  $X=0.8$ . At this value, the typical behavior is repeated, where the PDF uncertainty drops rapidly to 0.

The X uncertainty is also similar to what has been observed above. The band increases exponentially, again around  $X=0.003$ . In this case, this does not correspond to any special correlation coefficient. As always, our data is summarized in the following table for CT10w.

Table 4

CTEQ10w data for the transverse mass, momentum, and missing energy. The data is divided into sections based on the data shown in Figs. 12-14.

Quantity	Outlier PDF pair(s)	Max value correlation coefficient and position (abs. value)	PDF Uncertainty behavior at correlation coefficient position	X Uncertainty behavior at correlation coefficient position	Magnitude of PDF uncertainty band at correlation coefficient position	Magnitude of X uncertainty band at correlation coefficient position
$m_t$	3 is the largest. 6 and 21 are also large.	-0.5 at roughly $X \approx 0.11$	The band increases and decreases in a sinusoidal pattern until $X \approx 0.11$ , where the band increases exponentially	Narrow band, increases exponentially. The band increases exponentially starting near $X=0.003$ .	The band undulates slightly. When we reach $X \approx 0.11$ , it increases exponentially. At $X=0.8$ , where the band is at a maximum	Roughly $0.06 \times 10^{-3}$ to $0.06 \times 10^{-3}$ , reaching a maximum at $X=0.8$ from 1.5 to 1.5.



$p_t$	8 is the largest. 5 and 20 are also large.	-0.5 at $X=0.003$ , -0.3 at roughly $X \approx 0.11$ .	The band increases and decreases in a sinusoidal pattern until $X \approx 0.11$ , where the band increases exponentially	Narrow band, increases exponentially. The band increases exponentially starting near $X=0.003$ .	from -1.9 to 1.9. The band undulates slightly. When we reach $X \approx 0.11$ , it increases exponentially. At $X=0.8$ , where the band is at a maximum from -1.9 to 1.9.	Roughly -0.0005 to 0.0005. At $X=0.003$ , the band increases exponentially until we hit $X=0.8$ with a max width from -1.5 to 1.5.
$E_t$	3 is the largest. 11 is also somewhat large.	-0.2 at $X \approx 0.11$ . This is a very slight maximum.	The band increases and decreases in a sinusoidal pattern until $X \approx 0.11$ , where the band increases exponentially	Narrow band, increases exponentially. The band increases exponentially starting near $X=0.003$ .	The band undulates slightly. When we reach $X \approx 0.11$ , it increases exponentially. At $X=0.8$ , where the band is at a maximum from -1.9 to 1.9.	Roughly -0.0005 to 0.0005. At $X=0.003$ , the band increases exponentially until we hit $X=0.8$ with a max width from -1.5 to 1.5.

*III.a.4. CT10*

Like CT10w, CT10 has 53 eigen-values, 52 of which partition into 26 eigenvalue-pairs. As before, each eigenvalue-pair represents a specific parameter, and depending on which quantity we analyze, certain parameters will have larger error values. Unlike CT10w, CT10 does not take into account the  $W$  charge asymmetry. We will analyze our data as we did above, beginning with the transverse mass.

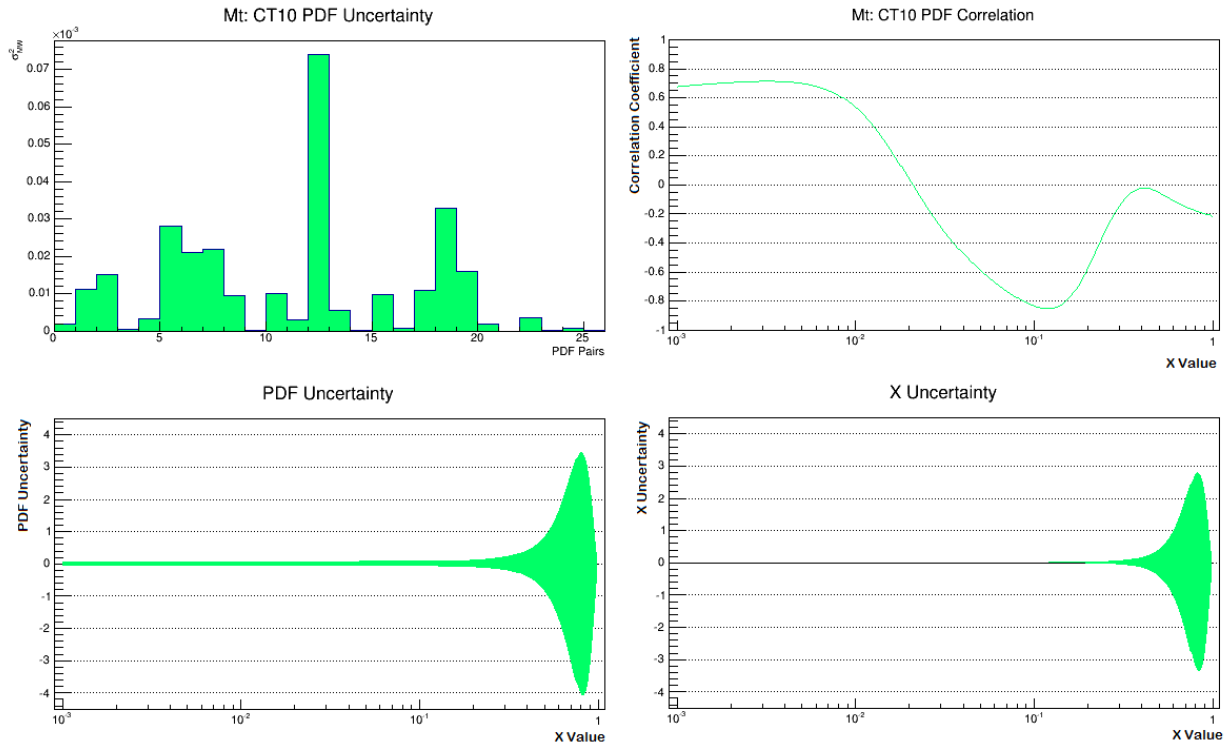


Figure 15: CT10 data for the transverse mass. Each graph represents similar data, as we discussed in CTEQ6.6 and CT10w above.

Eigenvalue-pair 13 is the major outlier in this case, followed closely by eigenvalue-pairs 19 and 6. Eigenvalue-pair 13 outstrips these in magnitude by nearly double; it is safe to say that it is the major contribution

to our overall uncertainty. There is a very slight maximum roughly near  $X=0.003$ , with a correlation coefficient of 0.7. This value drops very quickly, reaching a distinct maximum excursion near  $X=0.1$  with a coefficient of -0.9. The curve then bumps slightly and trails off, terminating when  $X=1.0$ .

If we look at these corresponding  $X$  values on the PDF and  $X$  uncertainty distributions, we observe interesting relations. Near  $X=0.1$ , the PDF uncertainty begins to expand rapidly, reaching a maximum value at  $X=0.8$  that stretches from roughly -4.0 to 3.5. Before this, the band undulates slightly as we saw above; there is no significant correlation between the  $X=0.003$  and the behavior of the PDF uncertainty distribution, although this  $X$  value does correspond to a maximum correlation coefficient.

The  $X$  uncertainty displays different phenomenon. It remains steady from  $X=0$  to roughly  $X=0.003$ , at which point it increase rapidly to a maximum band width from roughly -3.5 to 2.8, corresponding to a large correlation coefficient. Before this, the  $X$  uncertainty is steady in magnitude with a width from -0.06 to 0.06. In both the PDF and  $X$  uncertainty distributions, the bands drop steadily after  $X=0.8$  and fall to zero at  $X=1$ .

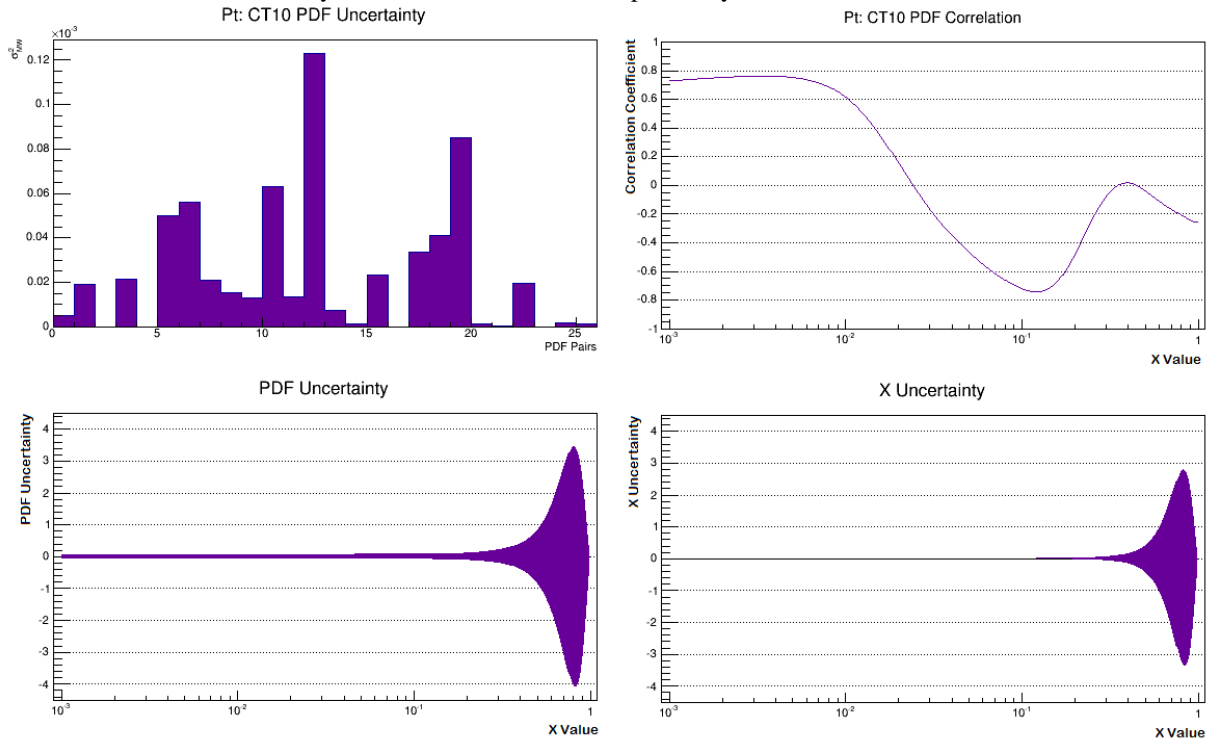


Figure 16: CT10 and the transverse momentum data.

There are more PDF outlier pairs in this case than the case above. The largest is eigenvalue-pair 13, followed by eigenvalue-pair 20. The PDF correlation displays the same behavior as was discussed above for the transverse mass. Near  $X=0.003$ , the correlation coefficient is roughly 0.8, presenting us with the highest value in this curve. Another point of interest is slightly past  $X=0.1$ , where the correlation coefficient reaches a maximum excursion value of roughly -0.7.

If we choose to analyze these points of interest on the PDF and  $X$  uncertainty distributions for any kind of relation, we find some interesting results. The PDF uncertainty reveals similar results; the band begins to increase exponentially slightly past  $X=0.1$ , indicating a correlation. This band reaches a maximum value at  $X=0.8$ , stretching from -4.0 to 3.5. The  $X$  uncertainty reaches a maximum at  $X=0.8$  as well, stretching from -3.5 to 2.8. At  $X=0.003$ , the band goes from being quite steady in value to increasing very rapidly in both distributions. As before, the PDF uncertainty undulates slightly, while the  $X$  uncertainty does not.

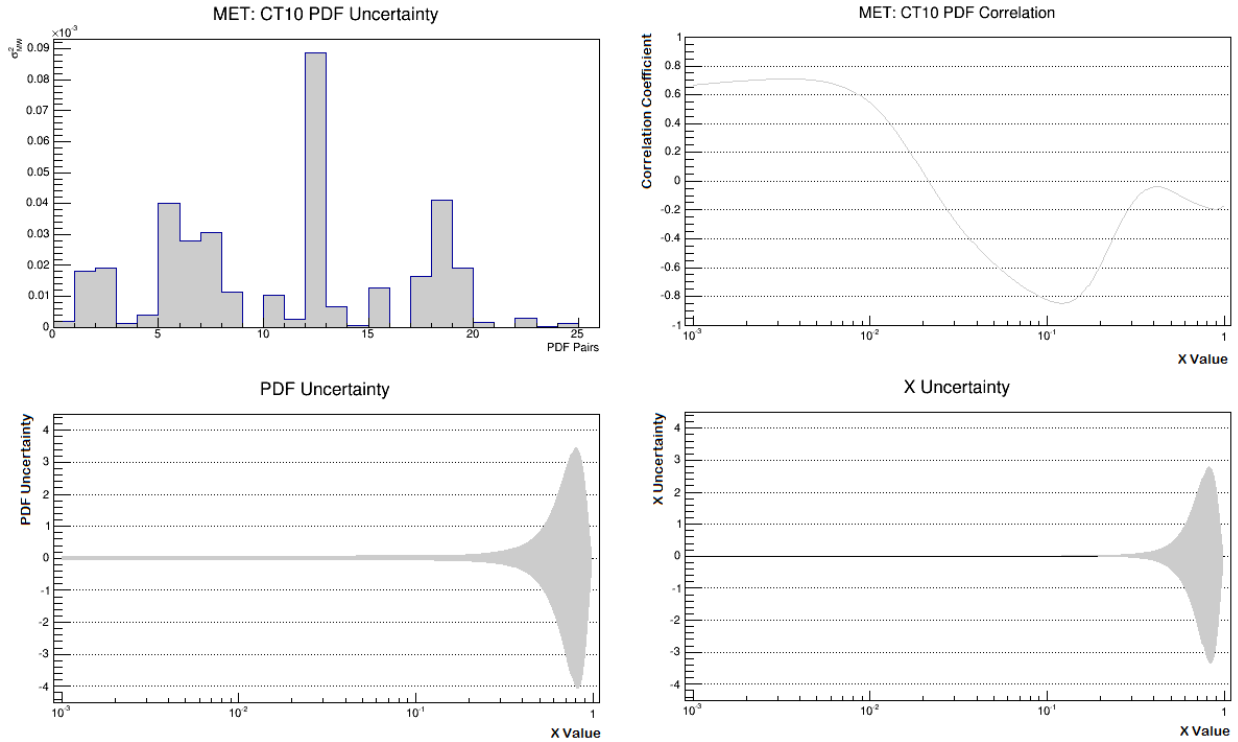


Figure 17: CT10 missing transverse energy data.

Eigen- pair 13 is a major outlier. Following this, eigenvalue-pairs 19 and 6 seem very close in magnitude. Due to their size, these eigenvalue-pairs influence the data more forcefully when we attempt to define the uncertainty. The correlation coefficient is roughly -0.9 at  $X=0.1$ , which is the maximum excursion value of the curve. Near  $X=0.003$ , the curve reaches a second high point, roughly 0.7. The behavior of the PDF and X uncertainty are nearly identical to those described above, so its description is relegated to the table below.

Table 5

CT10 data for the transverse mass, momentum, and missing energy. The data is divided into sections based on the data shown in Figs. 15-17.

Quantity	Outlier PDF pair(s)	Max value correlation coefficient and position (abs. value)	PDF Uncertainty behavior at correlation coefficient position	X Uncertainty behavior at correlation coefficient position	Magnitude of PDF uncertainty band at correlation coefficient position	Magnitude of X uncertainty band at correlation coefficient position
$m_t$	Eigenvalue -pair 13 is the largest, followed by eigenvalue -pairs 19 and 6.	-0.9 at $X \approx 0.11$ .	The band increases and decreases in a sinusoidal pattern until $X \approx 0.11$ , where the band increases exponentially.	Narrow band, increases exponentially. The band increases exponentially starting near $X=0.003$ .	The band undulates slightly. When we reach $X \approx 0.11$ , it increases exponentially. At $X=0.8$ , where the band is at a maximum from -4.0 to 3.5.	Roughly - $0.06 \times 10^{-3}$ to $0.06 \times 10^{-3}$ , reaching a maximum at $X=0.8$ from -3.5 to 2.8.
$p_t$	Eigenvalue -pair 13 is the largest, followed by eigenvalue	0.8 at $X=0.003$ , followed closely by -0.7 at $X \approx 0.11$ .	The band increases and decreases in a sinusoidal pattern until $X \approx 0.11$ , where	Narrow band, increases exponentially. The band increases exponentially	The band undulates slightly. When we reach $X \approx 0.11$ , it increases	Roughly - $0.06 \times 10^{-3}$ to $0.06 \times 10^{-3}$ , reaching a maximum at $X=0.8$ from -

	-pair 20.		the band increases exponentially.	starting near X=0.003.	exponentially. At X=0.8, where the band is at a maximum from -4.0 to 3.5.	3.5 to 2.8.
$E_t$	Eigenvalue -pair 13 is the largest, followed by eigenvalue -pairs 19 and 6.	0.7 at X=0.003, followed by -0.9 at X≈0.11.	The band increases and decreases in a sinusoidal pattern until X≈0.11, where the band increases exponentially.	Narrow band, increases exponentially. The band increases exponentially starting near X=0.003.	The band undulates slightly. When we reach X≈0.11, it increases exponentially. At X=0.8, where the band is at a maximum from -4.0 to 3.5.	Roughly $-0.06 \times 10^{-3}$ to $0.06 \times 10^{-3}$ , reaching a maximum at X=0.8 from -3.5 to 2.8.

III.a.5. CT10 [12]

Our last and final PDF set is the same as the PDF version just analyzed. CT10 [12] uses the same parameters as CT10, but with one exception.

Because of the exceedingly probable creation of a W boson from an up and down quark (and their anti-quarks), CT10 [12] is designed to focus primarily on collisions involving them, ignoring other flavors. They prove valuable because they are the most likely to occur. It is true that the W boson can be produced with other quark combinations, and the other three PDF sets analyzed above took these into account. In this case, we utilize something called the “CKM Matrix.” This matrix represents each quark with a number in the following way:

$$\begin{pmatrix} u & c & t \\ d & s & b \end{pmatrix} \leftrightarrow \begin{pmatrix} 1 & 4 & 6 \\ 2 & 3 & 5 \end{pmatrix}.$$

As can be seen here, the up and down quark collision that produces a W can be represented by the number 12. As such, if we “turn off” all the other elements of this matrix and focus primarily on the first two elements in column 1, we would obtain data pertaining only to the up and down quark. In ResBos, we restrict the production to u and d quarks by setting the CKM elements of all other flavors to zero.

CT10 [12] behaves in all other regards like CT10w and CT10. CT10 [12] has 53 eigen-values and 52 that form 26 total eigenvalue-pairs, each of which represents a parameter with inherent uncertainty. These are represented in the Figs. below as a histogram, telling us which parameter contributes to the uncertainty on  $M_W$  and by what amount. As always, we begin our analysis with the transverse mass.

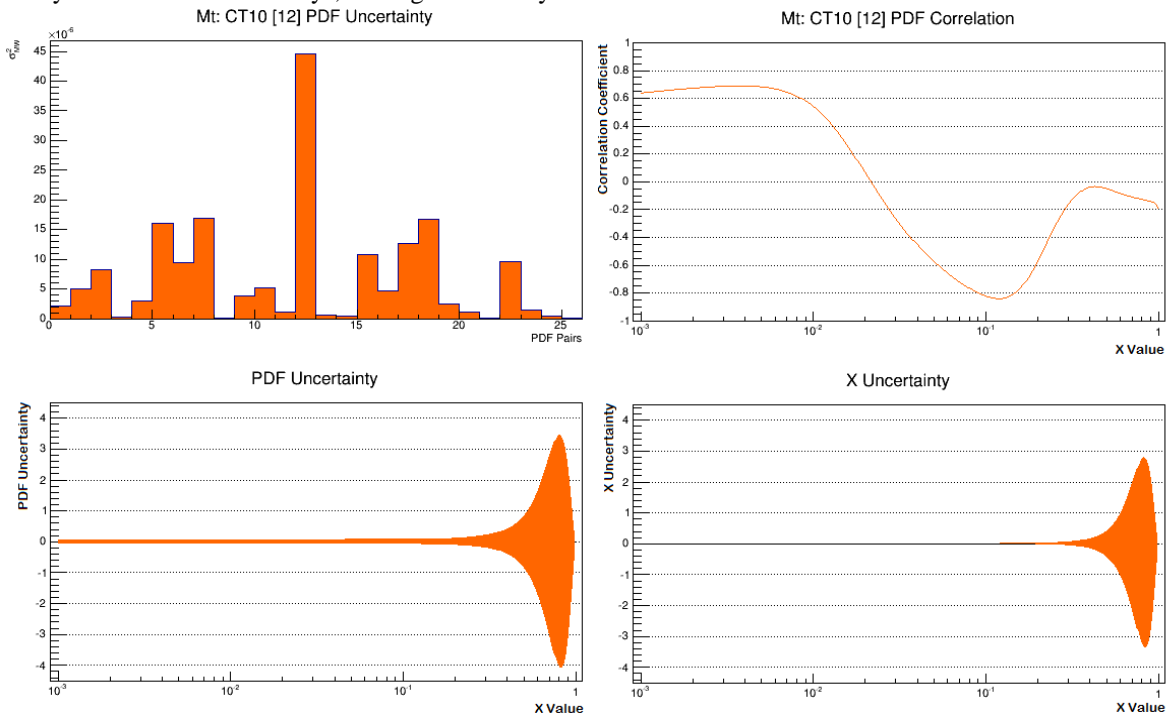


Figure 18: CT10 [12] transverse mass data.

In this case, it seems the 13<sup>th</sup> eigenvalue-pair is by far the largest, representing an enormous outlier. No other eigenvalue-pair comes close, which means the parameter 13 is dominant in its contribution to the uncertainty of  $M_W$ . As for the correlation coefficient, we again see a very large negative value roughly near  $X=0.1$ , which corresponds to a coefficient of roughly -0.85. In addition, near  $X=0.005$ , there is a slight increase, where the correlation coefficient reaches a value of roughly 0.7. As we did above, discussion of the behavior of the PDF and X uncertainties will be left to the table at the end of this section; the behavior is very similar to that described above for the CT10w and CT10 PDF sets.

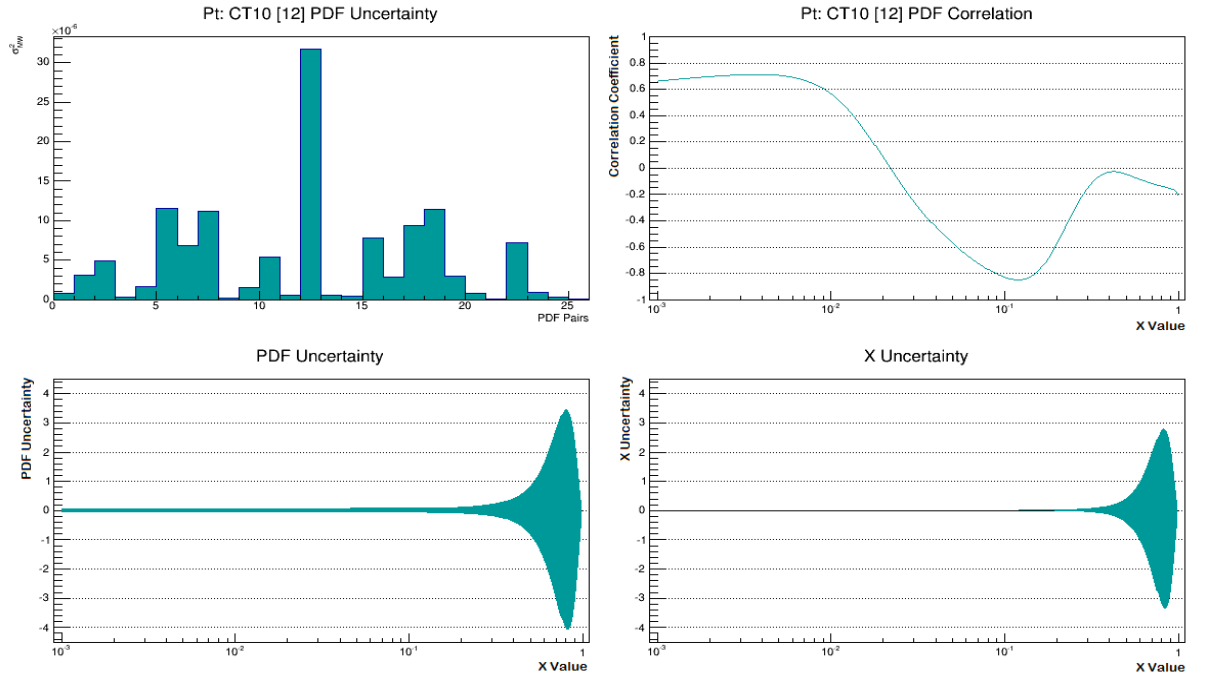


Figure 19: CT10 [12] transverse momentum data.

The transverse momentum shares an outlier with the transverse mass; eigenvalue-pair 13 is again an extremely large outlier. No other outlier come close in magnitude, again meaning that eigenvalue-pair 13 is exceedingly important in our  $M_W$  uncertainty. In addition, the correlation coefficient also reaches maxima in similar spots. A value of -0.85 is reached at  $X=0.1$ , while a second maximum is reached near  $X=0.005$ , with a value of roughly 0.7. The table below describes the behavior of the PDF and X uncertainty distributions.

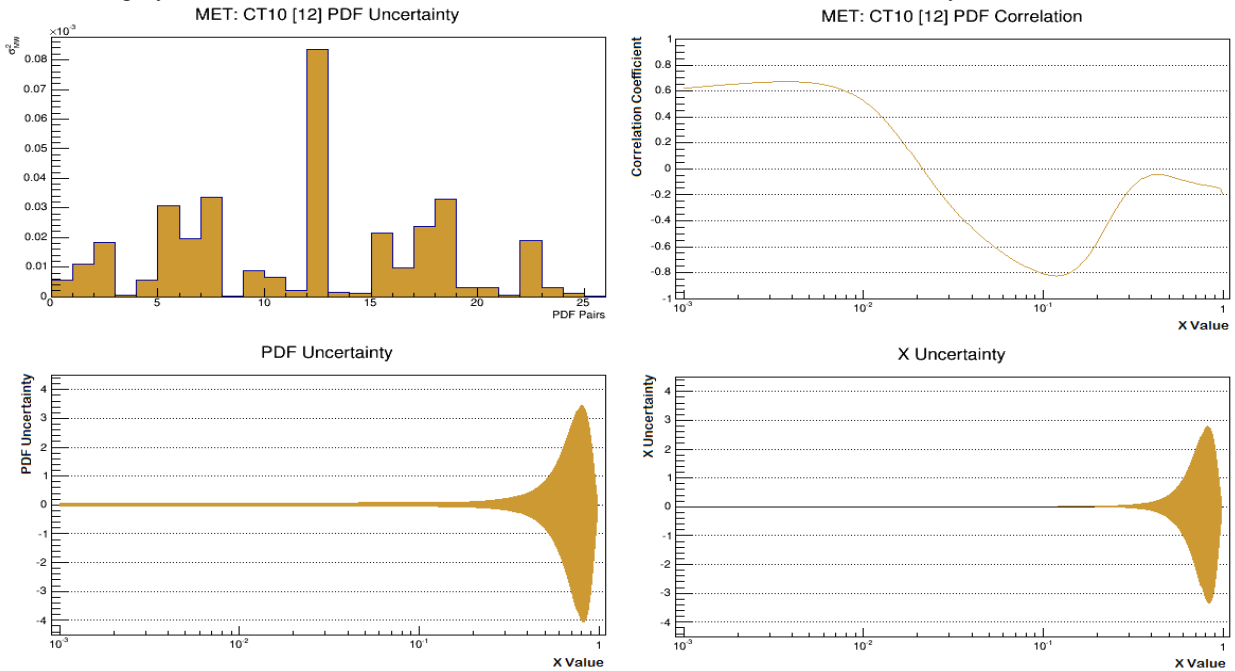


Figure 20: CT10 [12] missing transverse energy data.

Eigenvalue-pair 13 is an outlier yet again, and by a fairly significant margin. Like CTEQ6.6, CT10 [12] evidently only has one pair that truly matters in our determination of  $M_W$ ; this is quite different from the CT10w and CT10 cases, where a few eigenvalue-pairs were notable in magnitude. The correlation coefficient also behaves identically to the cases above: it reaches roughly  $-0.85$  at  $X=0.1$ , while a secondary maximum of  $0.7$  is reached at  $X=0.005$ .

*Table 6*  
 CT10 [12] data for the transverse mass, momentum, and missing energy. The data is divided into sections based on the data shown in Figs. 18-20.

Quantity	Outlier PDF pair(s)	Max value correlation coefficient and position (abs. value)	PDF Uncertainty behavior at correlation coefficient position	X Uncertainty behavior at correlation coefficient position	Magnitude of PDF uncertainty band at correlation coefficient position	Magnitude of X uncertainty band at correlation coefficient position
$m_t$	13	$-0.85$ at $X \approx 0.11$ , followed by $0.7$ at $X=0.005$ .	The band increases and decreases in a sinusoidal pattern until $X \approx 0.11$ , where the band increases exponentially.	Narrow band, increases exponentially. The band increases exponentially starting near $X=0.002$ .	The band undulates slightly. When we reach $X \approx 0.11$ , it increases exponentially. At $X=0.8$ , where the band is at a maximum from $-4.2$ to $3.5$ .	Roughly $0.06 \times 10^{-3}$ to $0.06 \times 10^{-3}$ , reaching a maximum at $X=0.8$ from $-3.5$ to $2.8$ .
$p_t$	13	$0.7$ at $X=0.005$ , followed closely by $-0.85$ at $X \approx 0.11$ .	The band increases and decreases in a sinusoidal pattern until $X \approx 0.11$ , where the band increases exponentially.	Narrow band, increases exponentially. The band increases exponentially starting near $X=0.002$ .	The band undulates slightly. When we reach $X \approx 0.11$ , it increases exponentially. At $X=0.8$ , where the band is at a maximum from $-4.2$ to $3.5$ .	Roughly $0.06 \times 10^{-3}$ to $0.06 \times 10^{-3}$ , reaching a maximum at $X=0.8$ from $-3.5$ to $2.8$ .
$E_t$	13	$0.7$ at $X=0.005$ , followed closely by $-0.85$ at $X \approx 0.11$ .	The band increases and decreases in a sinusoidal pattern until $X \approx 0.11$ , where the band increases exponentially.	Narrow band, increases exponentially. The band increases exponentially starting near $X=0.002$ .	The band undulates slightly. When we reach $X \approx 0.11$ , it increases exponentially. At $X=0.8$ , where the band is at a maximum from $-4.2$ to $3.5$ .	Roughly $0.06 \times 10^{-3}$ to $0.06 \times 10^{-3}$ , reaching a maximum at $X=0.8$ from $-3.5$ to $2.8$ .

**III.b. Interpretative Summary**

These results allow us to understand what factors predominantly contribute to the uncertainty on  $M_W$  arising from our four PDF sets, and where in parton momentum phase space these contributions arise. We must keep in mind the definition of a PDF set: it is a parton distribution function that represents the quark and anti-quark pairs being collided and contains within it a series of parameters used to determine  $M_W$  and its uncertainties. We have chosen to analyze four different versions using this functional approach to understanding  $M_W$ ; these are CTEQ6.6, CT10w, CT10, and the special case of CT10 [12].

When we analyze the data corresponding to CTEQ6.6, we find a very loose, if not completely nonexistent, correlation between the magnitude of the correlation coefficient given by equation [17] and the

magnitude of the PDF or X uncertainties in the missing transverse energy, transverse momentum, and transverse mass observables. We know this because the behavior of the PDF and X “uncertainty bands” does not significantly change at the corresponding x-axis position of the maximum absolute value of the correlation coefficient. Of the 22 eigenvalue-pair parameters that contribute most to this overall error regardless of its relation to the PDF and X uncertainties, parameter 12 is by far the most relevant. The maximum correlation coefficient occurs at  $X=0.1$  in all three cases, but the exponential-like increase we observe in each case does not correspond to this value. This implies that the correlation between the PDF set intrinsic uncertainty and the  $M_W$  error incurred is indirect.

In the case of CT10w, our measurements take into account the asymmetry of the W charge. There are 26 eigenvalue-pair parameters to account for in this case. An analysis of the correlation coefficient shows that the maximum is reached at roughly  $X \approx 0.11$  in all three cases. The relationship here between this extremized correlation coefficient and the PDF and X uncertainty bands is a bit more complex. In the transverse mass case, the correlation coefficient reaches a largest value of -0.5. At the X value in question, the PDF uncertainty begins to increase exponentially almost immediately; in addition, before this occurs, the PDF uncertainty undulates in magnitude in a sinusoidal fashion. The X uncertainty, however, does not appear to be correlated nearly as strongly, with an exponential increase occurring much earlier than expected. In the transverse mass case, the parameters that contribute most strongly to the uncertainty on  $M_W$  are pairs 3, 6, and 21. The transverse mass behaves similarly, but there are two correlation coefficients that are close in magnitude. At  $X=0.003$ , the value is -0.5 and near  $X \approx 0.11$  the value is 0.3. The PDF uncertainty band behaves sinusoidally until reaching  $X \approx 0.11$ , where it promptly increases exponentially. The X uncertainty, however, remains narrow until reaching  $X=0.003$ , at which point it too begins to increase exponentially. The pairs that contribute most in this case are 8, 5, and 20. Finally, we must consider the missing transverse energy case. Here, the correlation coefficient is decidedly flat in nature, reaching a rather shallow maximum of -0.2 at  $X \approx 0.11$ . The PDF uncertainty exhibits the same behavior described above at the X value in question, while the X uncertainty exhibits no observable correlation to X. The parameters that contribute most to the uncertainty on  $M_W$  are 3 and 11.

Evidently, there is a connection in the CT10w case between the correlation coefficient reaching a maximum and the PDF uncertainty band increasing rapidly. Meanwhile, the X uncertainty band is only correlated to the correlation coefficient in the transverse momentum case, and not the others. There uncertainty on  $M_W$  predicted by CT10w is thus directly related to the correlation coefficient.

CT10 also contains 26 eigenvalue-pair parameters as well, and we see some striking similarities between the behavior of this PDF set and CT10w. In all three cases, there is a correlation coefficient maximum at  $X \approx 0.11$ . In addition, in the transverse momentum and missing transverse energy cases there is a second maximum of noticeable magnitude at  $X=0.003$ . In the transverse mass case, we observe that parameter 13 contributes most to the uncertainty, followed by eigenvalue-pairs 19 and 6. We also notice that the PDF uncertainty band again increases exponentially at  $X \approx 0.11$ , where the correlation coefficient is maximized at a value of -0.9, after distinct sinusoidal behavior beforehand. The X uncertainty does not appear to be correlated to this maximized correlation coefficient in this case. In the transverse momentum case, it is interesting to note that while  $X \approx 0.11$  is a distinct correlation coefficient maximum, (value 0.7) it is not the largest.  $X=0.003$  is larger by a bit, reaching a magnitude of 0.8. The PDF uncertainty band follows the same exact behavior described above in the transverse mass case, while the X uncertainty band remains tight and narrow until 0.003, at which point it increases at an exponential rate. The largest eigenvalue-pairs in this instance are given by parameter 13 and parameter 20. Finally, considering the missing transverse energy case, we see that there are again two rather large correlation coefficients: one at  $X=0.003$  with a magnitude of 0.7, and another at  $X \approx 0.11$  with a magnitude of -0.9. The PDF uncertainty band behaves exactly as it did in both of the cases discussed above. The X uncertainty band exhibits the same behavior as was found in the transverse momentum case. The missing transverse energy has large eigenvalue-pair uncertainties at parameters 13, 19 and 6.

CT10 seems to be very strongly correlated to the maximization of the correlation coefficient in all three observable cases. In fact, it seems a direct pattern has been established. Each time the correlation coefficient became large, the PDF uncertainty band began to grow very rapidly. The X uncertainty band also exhibited this same behavior, but only in the transverse momentum and missing energy cases. CT10 is obviously directly affected by the correlation coefficient’s magnitude and the momentum ratio values where this occurs, as described by equation (17).

Finally, we discuss the special case of CT10 where only collisions between the up and the down quark (or their anti-quark pairs) are considered. As we have discussed, this specific PDF set is of particular importance to us because of the probable creation of a W boson from these constituent partons. In the transverse mass case, a maximum correlation coefficient occurs at two locations: at  $X \approx 0.11$  with a magnitude of -0.85, and at  $X=0.005$  with a magnitude of 0.7. The PDF uncertainty band correspondingly jumps exponentially at  $X \approx 0.11$  after the characteristic sinusoidal behavior we have come to expect occurs. The X uncertainty band, however, does not appear to be correlated in any way, as the exponential increase begins to occur at an unrelated X value.

The largest eigenvalue-pair parameter contributing to the uncertainty here is eigenvalue-pair 13. In the transverse momentum case, there are again two observable correlation coefficient maxima. At  $X \approx 0.11$ , the coefficient reaches its extreme value of 0.85, while at  $X = 0.005$ , it reaches a second extreme value of 0.7. The PDF uncertainty band behaves exactly the same as it did in the aforementioned case, while the X uncertainty again remains completely unrelated. The only eigenvalue-pair parameter to contribute a significantly large uncertainty in this case is again parameter 13. The missing transverse energy behaves similarly. There are two maxima here as well, again at  $X \approx 0.11$  and  $X = 0.005$  with values 0.85 and 0.7, respectively. The PDF uncertainty band mimics the behavior of the two cases previously discussed, while the X uncertainty band again remains uncorrelated. Eigenvalue-pair 13 is again the largest outlier parameter in this case.

It seems CT10 [12] is related to the correlation coefficient reaching a maximum value, but in a much looser sense than CT10 seemed to indicate. While the PDF uncertainty band definitely has a direct relation, the X uncertainty band does not. As such, we must conclude that in this special case, the PDF uncertainty band and the related uncertainty it confers onto our determination of  $M_W$  is certainly an observable direct relationship, while the X uncertainty remains a non-factor.

#### **IV. Conclusion**

The conclusions of this experiment with regards to the uncertainty induced on our determinations of  $M_W$  depend on the PDF set being used. As we saw, each PDF set has an inherent uncertainty that will be conferred on our overall W boson mass uncertainty determination, which is directly related to the parameter(s) that are exceptional outliers. We know that each parameter represents a different variable that can contribute uncertainty, so this allows us to discover which variables are skewing our results.

In addition, the correlation coefficient lets us find where the data relates most directly to the overall measurement of  $M_W$ . As such, if we locate where this coefficient has the largest magnitude- that is, where it is the most correlated to the data- we can find if this corresponds to a large uncertainty in the PDF or in X itself. Knowing this allows us to find which momentum ratio values, given by equation (17), will contribute the most uncertainty to our final  $M_W$  measurement.

As we saw, CTEQ6.6 does not provide us with any indication that maximizing the correlation coefficient affects the PDF or X uncertainty bands. CT10w had a strong connection between coefficient maximization and the PDF uncertainty band, but this connection was lost in the X uncertainty band case, with the exception of the transverse momentum case. CT10 was more exaggerated in its related behavior. Again, the PDF uncertainty band was correlated to maximization of the correlation coefficient in all three cases, but the X uncertainty band was only correlated in the transverse momentum and missing transverse energy cases. Finally, CT10 [12] indicated a much smaller uncertainty connection. While, again, the PDF uncertainty band was directly related by our observations, it seems the X uncertainty band was not in all three cases. This indicates a much looser connection than the generalized CT10 PDF set indicated.

##### **IV.a. Implications and Closing Remarks**

Each PDF set relates to the uncertainty on  $M_W$  in a slightly different way. For all but one set, the PDF uncertainty seems to directly relate to the correlation coefficient being at its largest absolute value. The same cannot be said for the X uncertainty. CTEQ6.6 seems to be the exception in this regard, because it behaves much differently than the other sets we have studied. Possible reasons for this exceptional behavior might have to do with the exceedingly large outlier presented by PDF parameter 12. This overwhelming uncertainty might dominate other potential sources of error, which obfuscates our ability to make more discrete predictions.

Overall, this data is quite valuable. Improving the uncertainty of the W boson mass correlates to a restriction on the mass of the Higgs boson. It also allows us to validate the standard model, which has acted as a guiding tool in our attempts to understand and predict the particle world and the behavior of its constituents as a whole. As such, this information should be taken and understood in a wider context, and as a simple experiment among a set of experimental constraints allowing us to further refine our model.

#### **References**

- [1] "The Standard Model of Particle Physics," M. Gaillard, P. Grannis, & F. Sciulli, Nov. 20, 1998. Published in *Reviews of Modern Physics*, 71 (1999) S96-S111. <http://inspirehep.net/search?p=find+eprint+HEP-PH/9812285>.
- [2] "Measurement of the W Boson Mass with the D0 Detector," Published in *Physical Review Letter* 108, 151804 (2012). <http://link.aps.org/doi/10.1103/PhysRevLett.108.151804>.
- [3] "The Upgraded D0 Detector," Published in *Nuclear Instruments and Methods A* 565:463-537 (2006). <http://arxiv.org/abs/physics/0507191>.
- [4] "Study of CP-violating charge asymmetries of single muons and like-sign dimuons in p pbar collisions," Submitted to *Physical Review D*. <http://arxiv.org/abs/1310.0447>.